FELIPE ARDITTI

Thrust allocation algorithm considering hydrodynamic interactions and actuator physical limitations

São Paulo
2019

FELIPE ARDITTI

THRUST ALLOCATION ALGORITHM CONSIDERING HYDRODYNAMIC INTERACTIONS AND ACTUATOR PHYSICAL LIMITATIONS

Master Thesis presented to the Escola Politécnica, Universidade de São Paulo to obtain the degree of Master of Science.

São Paulo
2019

FELIPE ARDITTI

THRUST ALLOCATION ALGORITHM CONSIDERING HYDRODYNAMIC INTERACTIONS AND ACTUATOR PHYSICAL LIMITATIONS

Master Thesis presented to the Escola Politécnica, Universidade de São Paulo to obtain the degree of Master of Science.

Concentration area: Mechatronics Engineering

Advisor: Prof. Dr. Eduardo Aoun Tannuri

São Paulo
2019

Este exemplar foi revisado e corrigido em relação à versão original, sob responsabilidade única do autor e com a anuência de seu orientador.

São Paulo, 30 de junho de 2019

Assinatura do autor: 

Assinatura do orientador: _____

Catalogação-na-publicação

Arditti, Felipe
Thrust allocation algorithm considering hydrodynamic interactions and actuator physical limitations / F. Arditti -- versão corr. -- São Paulo, 2019.
120 p.

Dissertação (Mestrado) - Escola Politécnica da Universidade de São Paulo. Departamento de Engenharia Mecatrônica e de Sistemas Mecânicos.

1.Dynamic Positioning 2.Thrust Allocation 3.Hydrodynamic Interactions I.Universidade de São Paulo. Escola Politécnica. Departamento de Engenharia Mecatrônica e de Sistemas Mecânicos II.t.

ARDITTI, F. **Thrust Allocation Algorithm Considering Hydrodynamic Interactions and Actuator Physical Limitations**. São Paulo. 2019. 120 p. (Pós-Graduação) Escola Politécnica, Universidade de São Paulo, São Paulo, 2019.

À minha família

Brasileira e Holandesa

Que sempre me apoia.

To my Family

Dutch and Brazilian

Who always supports me.

Aan mijn familie

Nederlands en Braziliaans

Die ondersteunt me altijd.

AGRADECIMENTOS

Ao meu orientador, Prof. Dr. Eduardo Aoun Tannuri, com quem trabalho em alocação de empuxo desde 2010. Durante toda essa trajetória sempre me apoiou, incentivou e esteve disposto a ajudar, desde discussões técnicas até questões pessoais. Além de dividir comigo seu vasto conhecimento na área de controle de embarcações, foi de extrema importância na análise e preparação dos trabalhos publicados. Não obstante sou extremamente grato pela confiança depositada ao permitir que eu cursasse o mestrado enquanto trabalhava.

A Hans Cozijn e Ed van Daalen do Maritime Research Institute Netherlands (MARIN) pelo apoio nas publicações realizadas durante o mestrado.

Ao Prof. Dr. Thiago de Castro Martins pelas enriquecedoras discussões sobre otimização.

Aos colegas do TPN, Felipe Lopes de Souza com quem cursei matérias do mestrado e sempre se mostrou interessado em discutir o problema de alocação de empuxo, e André S. S. Ianagui com quem tive a oportunidade de apresentar no IFAC-CAMS 2018.

Finalmente, à minha família brasileira e holandesa pelo incentivo e altruísmo, pois realizei boa parte das atividades do mestrado no meu tempo com eles.

ABSTRACT

The Dynamic Positioning (DP) System is responsible for the station keeping of vessels in several offshore operations. The forces required by the DP System are distributed among the available thrusters by a thrust allocation algorithm which should be accurate, efficient and robust. This means that the effective forces match the required forces while power consumption is minimized. Additionally, in case of impossibility of generating the required forces the heading of the vessel is maintained to avoid increasing environmental forces. To accurately generate the required forces, the physical limitations of the thrusters and the hydrodynamic interactions must be considered. The hydrodynamic interactions are consistently modelled to accommodate the following typical effects: thruster-hull, thruster-current and thruster-thruster interaction. The result of this modeling is a nonlinear optimization problem, which is solved using the Sequential Quadratic Programming (SQP) algorithm with slack variables. The DP simulation carried out show that by considering the hydrodynamic interactions on thrust allocation the overall performance (controllability and power consumption) of the DP system is improved.

Key-words: Dynamic Positioning, Thrust Allocation, Hydrodynamic Interactions

RESUMO

O Sistema de Posicionamento Dinâmico (DP) é responsável pela manutenção da posição de embarcações em diversas operações offshore. As forças requeridas pelo Sistema DP são distribuídas entre os propulsores disponíveis por um algoritmo de alocação de empuxo que deve ser preciso, eficiente e robusto. Isso significa que as forças efetivas correspondem às forças solicitadas, enquanto o consumo de energia é minimizado. Além disso, em caso de impossibilidade de gerar as forças necessárias, o rumo da embarcação é mantido para evitar o aumento das forças ambientais. Para gerar com precisão as forças necessárias, as limitações físicas dos propulsores e as interações hidrodinâmicas devem ser consideradas. As interações hidrodinâmicas são modeladas de forma consistente para acomodar os seguintes efeitos típicos: interação entre casco e propulsor, correnteza e propulsor e entre propulsores. O resultado desta modelagem é um problema de otimização não linear, que é resolvido usando o algoritmo de Programação Quadrática Sequencial (SQP) com variáveis de relaxamento. As simulações de posicionameto dinâmico realizadas mostram que, ao considerar as interações hidrodinâmicas na alocação de empuxo, o desempenho geral (controlabilidade e consumo de energia) do sistema DP melhora.

Palavras-chave: Posicionamento Dinâmico, Alocação de Empuxo, Interações Hidrodinâmicas.

LIST OF FIGURES

LIST OF TABLES

LIST OF ABREVIATIONS

TPN – *Tanque de Provas Numérico* – Numerical Offshore Tank

DP – Dynamic Positioning

SQP – Sequential Quadratic Programming

SD – Steepest Descent

CFD – Computational Fluid Dynamics

FZ – Forbidden Zone

MPC – Model Predictive Control

PIV – Particle Image Velocimetry

QP – Quadratic Programming

NOMENCLATURE

Table A. 1 presents the name, the symbol and the unit of thruster variables.

Table A. 1 – Thruster variables.

Name	Symbol	Unit
Longitudinal position	x	$[m]$
Lateral position	y	$[m]$
Thruster diameter	D	$[m]$
Thruster velocity	n	$[s^{-1}]$
Maximum velocity of the Thruster	n_{max}	$[s^{-1}]$
Maximum acceleration of the propeller	$\dot{n}_{max}$	$[s^{-2}]$
Thruster azimuth angle	α	$[rad]$
Maximum rate of turn of the thruster azimuth angle	$\dot{\alpha}_{max}$	$\left[\frac{rad}{s}\right]$
Water density	ρ	$\left[\frac{kg}{m^3}\right]$
Current velocity	V_{cur}	$\left[\frac{m}{s}\right]$
Current angle of attack	γ_{cur}	$[rad]$
Advance ratio	J	$[-]$
Coefficient of advance velocity	β	$[rad]$
Thrust coefficient	C_T	$[-]$
Thrust coefficient in bollard pull	C_{T_B}	$[-]$
Torque coefficient	C_Q	$[-]$
Torque coefficient in bollard pull	C_{Q_B}	$[-]$
Thrust in open water and bollard pull condition	T_B	$[N]$
Thrust considering the inflow effect (thrust delivered)	T_d	$[N]$
Effective thrust	T_{eff}	$[N]$
Torque	Q	$[Nm]$
Power	P	$[W]$

Table A. 2 presents the information available for the thrust allocation.

Table A. 2 – Thrust Allocation variables.

Name	Symbol	Unit
Number of thrusters	N	$[-]$
Forces required	$\mathbf{F}_{req}$	$[N]$
Force required in surge direction	F_x	$[N]$
Force required in sway direction	F_y	$[N]$
Force required in yaw direction	M_z	$[Nm]$
Previous thrust	T_0	$[N]$
Previous azimuth angle	α_0	$[rad]$
Vessel heading	φ	$[rad]$

TABLE OF CONTENTS

1. INTRODUCTION

The oil and gas prices made economically viable the offshore exploration. For example, more and more oil platforms are moving towards Campos and Santos basin and the Mexican gulf. This growing movement led to the development of new technologies for offshore exploration.

In Brazil the movement was led by the state company PETROBRAS, which started to explore the offshore fields in Campos and Santos basin. For the offshore exploration, the most economically viable solution is assisting the operations, such as, drilling, offloading and pipe-laying with DP systems.

The DP is an alternative to the conventional mooring system, in situations in which it is neither possible nor economically feasible to moor the vessel. The DP system is responsible for the station keeping of the vessel. It uses the thrusters of the vessel to counterbalance the environmental loads (wind, current and waves) that act on it.

The DP systems available in the market do not consider the hydrodynamic interaction (thruster-hull, thruster-current and thruster-thruster) effects directly; generally, this is done by defining forbidden zones where strong interaction is likely to occur. Motivated by the current situation and the relevance of the hydrodynamic interaction phenomena, the THRUST JIP Project started in 2011, led by the MARIN institute, with the participation of 17 oil and gas, shipbuilding and research companies, including Petrobras, Daewoo and Rolls Royce.

This dissertation follows up the developments initiated in this project, when TPN-USP took part in the project with PETROBRAS. The development of a robust thrust allocation algorithm, taking into account the hydrodynamic interaction phenomena and physical limitation of the actuators, is capable of improving the DP system and the vessel’s capability (increasing the operational window) when performing offshore operations.

1.1. Motivation

Figure 1. 1presents the thrust allocation algorithm functionality within the DP System (further details are given in the theoretical background section). The control

system calculates the required forces in order to counterbalance the environmental loads that act on vessel. The thrust allocation algorithm optimally divides the required forces among the thrusters available in the vessel. Therefore, it defines the operational set points of the thrusters and sends this information to the low level thruster control.

Figure 1. 1– Thrust allocation algorithm function inside the DP System.

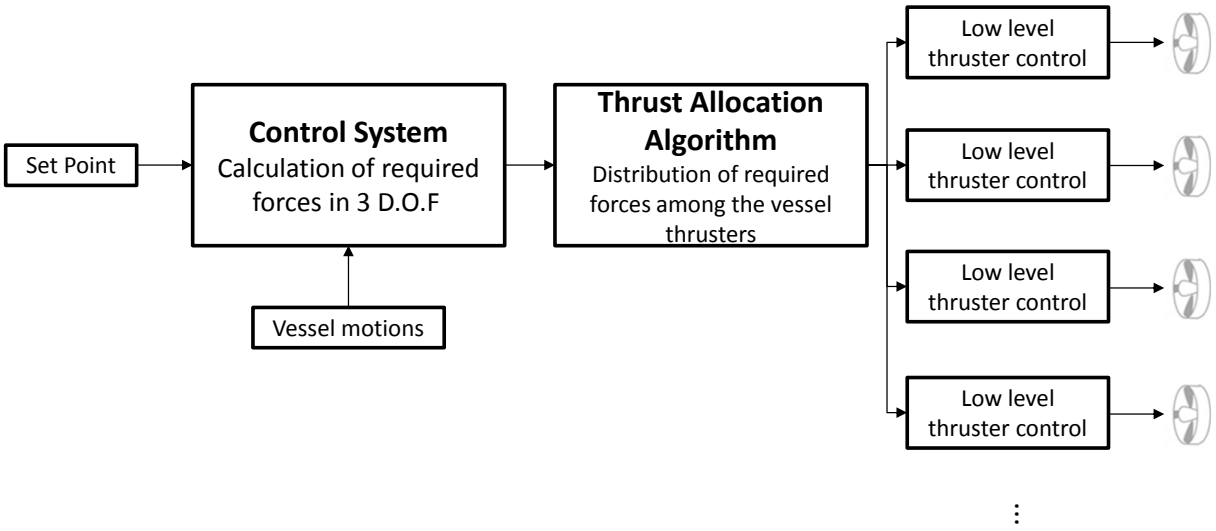

Source: Elaborated by the author.

In order to maintain the ship stationary during DP operations it is necessary to counterbalance the environmental forces that act on the vessel in surge, sway and yaw motions. There are three degrees of freedom involved in the problem. However, due to safety and better operability there are more thrusters than the minimum required, which configures an over actuated problem, subject to optimization.

The development of thrust allocation algorithms is a mature subject. A general review of allocation algorithms is available in Johansen and Fossen (2013). The main advances of the thrust allocation problem and the developed methods for solving it are briefly discussed as follows. The first characterization of the thrust allocation problem employed an approximative quadratic relation between thrust and power, resulting in a linear set of equations when using a Lagrange multiplier optimization method, which in simpler configurations is solved by the pseudo-inverse operation.

Examples of this solution can be found in Wei *et al.* (2013) and Shi-zhi, Wang, and Sun (2011).

The second step in the evolution of the thrust allocation problems was to use the exact relationship between thrust and power. Note that this relationship is valid for conditions in which the vessel is in a stationary condition, known as bollard pull. The solution for this problem can be obtained by means of the Newton-Raphson algorithm, as demonstrated in Van Daalen *et al.* (2011).

A significant increase in the complexity of the problem was introduced by considering the saturation of the thrusters, which leads to cases where it is not possible to generate the forces required by the control system. Different solutions were proposed to this problem: The reallocation procedure as described in Arditti *et al.* (2015) keeps the saturated thruster at its azimuth angle and maximum force, and a new allocation problem is solved without the saturated thruster and considering the forces developed by it as an external force. The addition of the errors in the required force constraints to the objective function (in order to minimize the errors) is presented in Arditti *et al.* (2014). The use of slack variables (Johansen, Fossen, and Berge 2004) is a powerful mathematical solution that relaxes the optimization problem and guarantees that a solution for the problem can always be found at the cost of a quadratic error, which should be minimized in the objective function.

Recent developments suggest implementing practical problems inside the thrust allocation, since this module could provide the best integrated solution. The thrust biasing is a technique in which two close by thrusters generate the required forces, by producing forces against each other, to guarantee that the minimum thrust necessary for its operation is used. This is necessary because the control of a thruster in low angular speed is not efficient and could cause a start-stop behavior leading to incorrect force generation. An example of the use of this technique is presented in Wen, Xu and Feng (2016).

The use of the thrust allocation algorithm to regulate the general power consumption of the vessel has also been suggested. It is an interesting approach since the thrust generation corresponds to more than 50% of the total power consumption of the vessel. The minimization of power variation by means of the thrust allocation is presented in Ding, Yang, and Huang (2016), whereas the

modulation of the vessel electric bus through thrust allocation is presented in Veksler *et al.* (2015).

The thrust allocation algorithm is also important in DP simulations of thrust failures. An investigation of the positioning performances for DP vessels considering thruster failure by a novel criterion is presented in Xu *et al.* (2017). An adaptive control system where the DP controller uses a back-stepping method and the thrust allocation is performed with SQP method is presented in Witkowska and Śmierzchalski (2018); the algorithm developed in this paper can adapt to unknown partial or total thrust failures, which configures a robust solution.

The incorporation of the thrust allocation problem within the vessel control system is presented in Veksler *et al.* (2016) as Model Predictive Control (MPC). In this approach, the dynamic equations of the vessel are merged with the usual force generation and power consumption equations of the thrust allocation problem. Specifically, the vessel is aimed to follow a pre-defined route with a maximum deviation constraint, minimizing the power consumption. Skjong and Pedersen (2017) implements a non-angular MPC algorithm, which significantly reduces the problem complexity and leads to a faster and more efficient solution.

Computational Fluid Dynamics (CFD) (Cozijn and Hallmann 2012) and model based (Arditti and Tannuri 2012) tests show that hydrodynamic interactions can drastically influence the net thrust. The work presented in Arditti *et al.* (2014) and Arditti *et al.* (2015), with some simplifications in the representation of hydrodynamic interaction, illustrates that by considering these phenomena in the thrust allocation higher reliability and minimization of power consumption can be achieved.

1.2. Objectives

The main objectives of this dissertation are:

1) Improving the model used for the hydrodynamic interactions. Although Arditti *et al.* (2014) presents a consistent approach for this problem, higher accuracy can be achieved by considering the effects of energy loss and radial speed of the wake flow of thrusters.

2) Providing a robust approach for the situation in which it is not possible to generate the required forces. Arditti *et al.* (2015) provides a solution for this problem, however with the need to perform multiple reallocations, which is not

efficient. Johansen, Fossen, and Berge (2004) provides an efficient solution for the reallocation problem, however this method is not yet tested in thrust allocation problems considering hydrodynamic interactions.

3) Performing time domain simulations of the developed thrust allocation algorithm, to evaluate the impacts of the improvements in the overall performance of the DP system.

1.3. Resources and Methods

To achieve the project objectives, the research is divided in two parts.

1.3.1. Modelling the Optimization Problem

This part of the research focuses in objective 1 and 2. By using data available in the bibliography (e.g. Cozijn and Hallmann 2012), which contains CFD and PIV simulations of the thruster wake flow, a better model for the thruster-thruster interaction can be developed. Furthermore, by incorporating slack variables to the thrust allocation structure (as in Johansen, Fossen, and Berge 2004), a robust solution for the problem can be obtained.

1.3.2. Performing time domain Simulations

The simulations are executed using the Dynasim, a time domain numerical simulator developed by Petrobras in co-operation with Brazilian universities. It was designed for the analysis of moored and DP offshore systems. The mathematical model of the Dynasim and validation results are presented in Nishimoto et al. (2002) and Tannuri and Morishita (2006), Tannuri et al. (2009). A customized version of the simulator is used, which allows the integration with specific control and allocation algorithms, enabling the investigation of the possible improvements that the developed thrust allocation algorithm can bring to the DP system.

1.4. Structure of the Text

The Theoretical Background chapter presents the stepping stones of this research, which are, the DP System, thrust allocation, hydrodynamic interactions,

and physical limitations of the thrusters. Overall, this chapter sets the foundation for all the following chapters.

The Thrust Allocation – State of the Art presents the evolution of the thrust allocation problem. It is organized in a way that the reader can understand from its basis up to latest improvements.

In the Modelling the Optimization Problem chapter, mathematical models are developed for representing hydrodynamic interactions, physical limitations, power consumption and effective thrust.

The Development of the Thrust Allocation Algorithm chapter presents several optimization techniques, which are discussed in order to select the best candidate considering the problem characteristics. The developed algorithm is presented with its structure and main functions.

The Case Study presents simulations of the developed thrust allocation algorithms, in time domain simulations. The results are discussed and compared with recent developments on thrust allocation.

To finalize the Conclusions Recommendations for Future Works are presented.

2. THEORETICAL BACKGROUND

2.1. Coordinate System and Variables

Figure 2. 1 presents the global and local coordinate systems. The global system is based in the North-End-Down (NED) basis, whereas the local system is based on the vessel surge, sway and yaw directions. The local coordinate system is used as the standard system throughout the text, if the global coordinate system is referred to, it will be explicitly detailed.

Figure 2. 1– Global and local coordinate system.

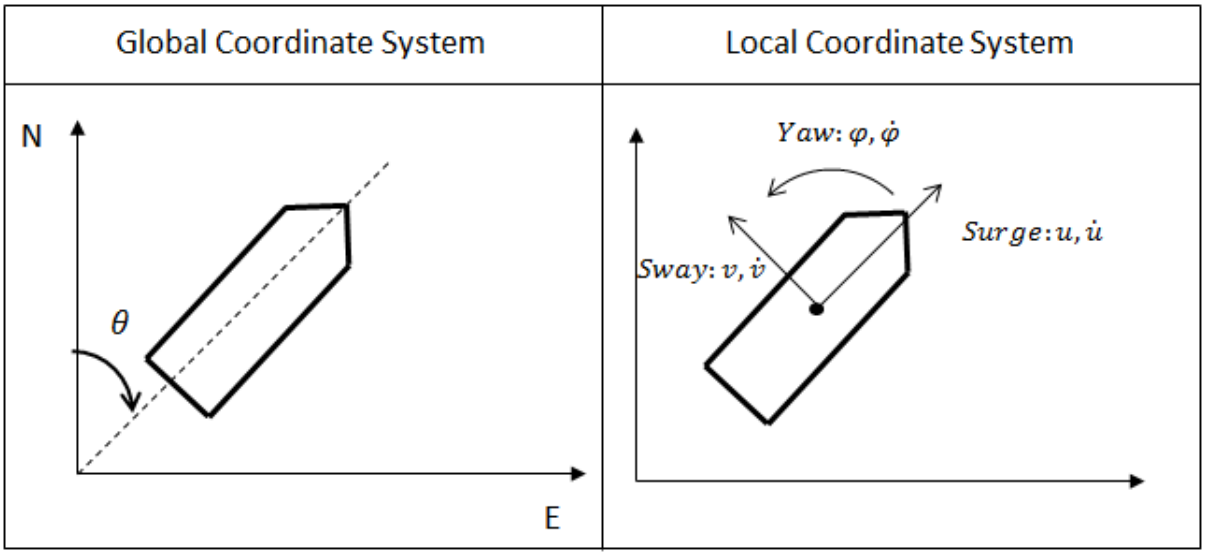

Source: Elaborated by the author.

It is also important to define the variables with respect to the thrusters. Figure 2. 2 presents the position of the thrusters with respect to the gravity center of the vessel (x_i, y_i), the developed thrust (T_i) and respective azimuth angle (α_i), and its decompostion in surge and sway directions (F_{x_i}, F_{y_i}).

Figure 2. 2 – Thruster variables.

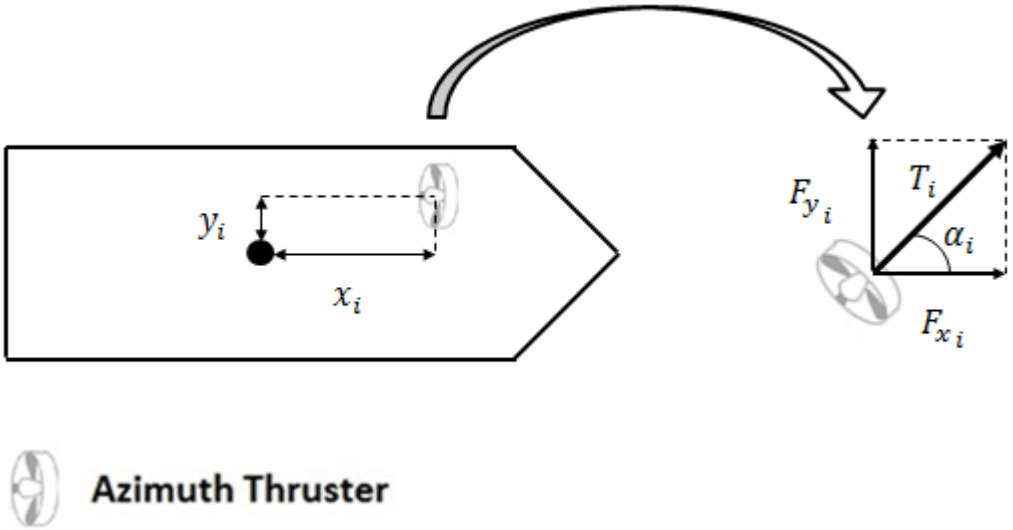

Source: Elaborated by the author.

2.2. DP System

With the offshore industry moving to ever deeper waters, more and more vessels are equipped with DP systems. On a DP vessel a feedback system controls the thrusters in order to keep the vessel in a desired position, thus eliminating the need for mooring lines.

The DP System is a technology that is highly required for offshore operations. It is an alternative to the conventional mooring system, in situations in which it is neither possible nor economically feasible to moor the vessel. The DP system is responsible for the station keeping of the vessel, thus allowing it to perform offshore operations, e.g. drilling, offloading, and pipe-laying

The DP system on board of the vessel contains several hardware and software components as shown in the schematic overview in Figure 2. 3. The main components of the DP system are briefly described. More detailed explanations can be found in e.g. Sorensen (2011) and Tannuri (2002).

Briefly, the DP system contains a **Control System** that receives a **Set Point** (which is the desired position and heading of vessel), the **Actual Position and Heading** of the vessel (data acquired by a DGPS and other position reference systems, and processed by a Kalman Filter to avoid response to wave frequent-motions) and in some cases a feed-forward of the wind load. The **Control System**

calculates the **Required Total Forces and Moment** to lead the vessel to its **Set Point**; a **Thrust Allocation Algorithm** distributes the **Required Total Forces and Moment** among the available actuators in such a way that the required power is minimal.

Figure 2. 3 – DP System.

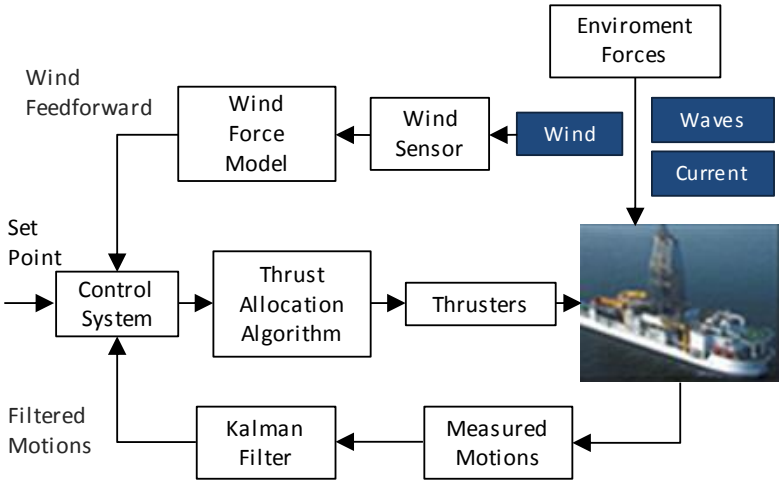

Source: Arditti, Cozijn and Van Daalen (2014).

Note that improvements in the thrust allocation algorithm would lead to enhancements of the DP system, since it is a task of main importance inside the DP structure.

According to the ABS GUIDE FOR DYNAMIC POSITIONING SYSTEMS (ABS 2013) the DP system is classified according to the following requirements:

- For a vessel with the notation DPS-0, or DPS-1, a loss of position may occur in the event of a single fault.
- For a vessel with the notation DPS-2, a loss of position may not occur in the event of a single fault in any active component or system, excluding a loss of compartment or compartments.

- For a vessel with the notation DPS-3, a loss of position may not occur in the event of a single fault in any active or static component or system, including complete loss of a compartment due to fire or flood.

Observe that the thrust allocation algorithm should be robust enough to guarantee the station keeping capability even with the fault of thrusters, in order to be classified as DPS-2 or DPS-3.

2.3. Thrust Allocation

The thrust allocation algorithm should distribute the required total forces and moment among the available thrusters with minimal use of power (Jenssen and Realfsen 2006), which means determining the thrust and azimuth angle of all the thrusters.

In order to guarantee the safety of the operation and to reach a better station keeping capability, the vessels usually have more thrusters than the minimum number of thrusters needed to generate the required forces. Therefore, the thrust allocation is a redundant problem with a non-unique solution. A review on allocation algorithms is available in Johansen and Fossen (2013). A simple graphical illustration of thrust allocation can be found in Arditti and Tannuri (2012). Further details on the developments of thrust allocation algorithms are presented in the Chapter 3.

2.4. Actuators

There are several models of actuators that produce thrust in a DP System. These actuators are classified according to their capacity of producing thrust in different directions. Table 2. 1 presents a short description of all kinds of actuators with the respective image.

Table 2. 1– Classification of Actuators.

Name	Image	Short Description
Main propeller	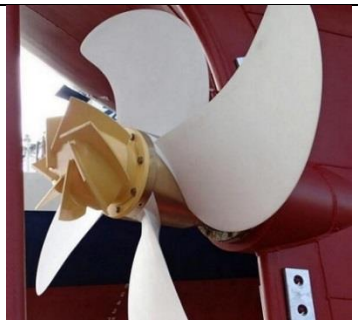 Source: Consolidated Training Systems Incorporated (2019).	The main propeller is able to produce thrust in surge direction. It is more efficient when it produces thrust forward.
Tunnel thruster	 Source: Marine Insight (2019).	The tunnel thruster is able to produce thrust in the sway direction.
Azimuth thruster	 Source:HighSea Marine (2019).	The azimuth thruster can produce thrust in any direction in the plane defined by surge and sway. It has two inputs, the thrust and the azimuth angle.
Main propeller with rudder	 Source: Kongsberg (2019).	The main propeller with rudder is capable of producing thrust in sway direction when it produces thrust forward, by controlling the angle of the rudder. The water jet slides through the rudder changing its direction and pushing the rudder both in surge and sway directions.

2.5. Hydrodynamic Interaction Effects

The objective of this section is to qualitatevely explain the main hydrodynamic interaction effects and how they occur.

2.5.1. Thruster-hull interaction

This interaction is caused mainly by the drag and pressure forces on the hull, due to the wake flow of the thrusters. It also includes the Coanda effect (change in the form of the thruster water jet according to the form of the hull) and the deflection of the water jet The thruster-hull interaction mainly depends on the form of the hull, in some cases on the pontoon of a platform (Figure 2. 4), other underwater equipment, and the thruster position. Recent studies demonstrate that the efficiency due to this interaction can drop by 40% (Cozijn and Hallmann, 2013). More details can be found in Ekstrom and Brown (2002).

Figure 2. 4– Thruster-hull interaction (wake flow clash with a pontoon).

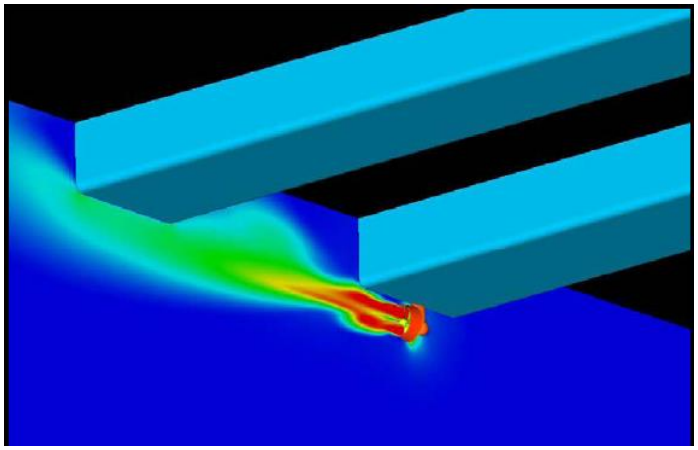

Source: Image courtesy of MARIN of a CFD study.

2.5.2. Thruster-Current Interaction

The thruster-current interaction affects the inflow current of the thrusters. It causes variation in the thrust and torque coefficients (C_T and C_Q), which will differ from its values in the bollard pull condition. Note that, the main property to investigate this phenomenon is the advance velocity of the thruster (J – dimensionless), which is the relative velocity between the blades of the thruster and the inflow current.

The change in the coefficients could be interpreted as a change in the state of the thruster. Any change in the thrust and torque coefficients has direct impact on the delivered thrust and consumed power. The four-quadrant diagram presented in Figure 2. 5 shows how the advance velocity ($\beta = arctg(J)$) affects the thrust and torque coefficients of the thruster. Note that the data in this figure is from tests with B-series propellers.

Figure 2. 5 – Thruster Four-Quadrant Diagram.

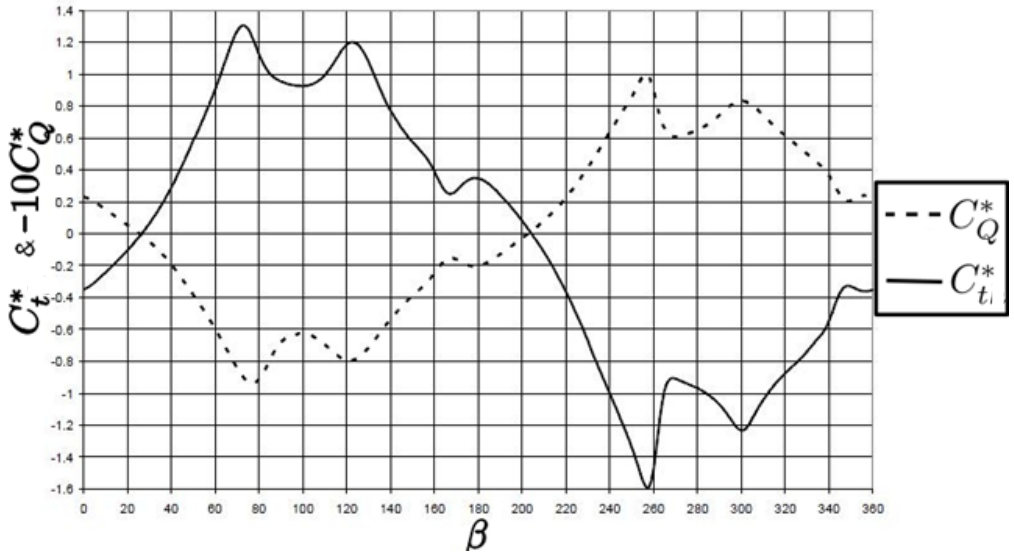

Source: Carlton (2007).

2.5.3. Thruster-Thruster Interaction

The interaction between thrusters is the most complex phenomenon. It can be seen as a combination of thruster-hull and thruster-current interaction. On the one hand, its nature is similar to the thruster-current interaction, which means it affects the inflow of the thrusters, changing the thrust and torque coefficients. On the other hand, the wake flow from one thruster clashes with the other thruster, generating a force in the direction of the wake flow. Observe that this phenomenon depends on every thruster azimuth angle and generated thrust; it can be influenced by the natural current and by the form of the hull. Figure 2. 6 presents a case of significant thruster-thruster interaction

Figure 2. 6 – Thruster-thruster interaction.

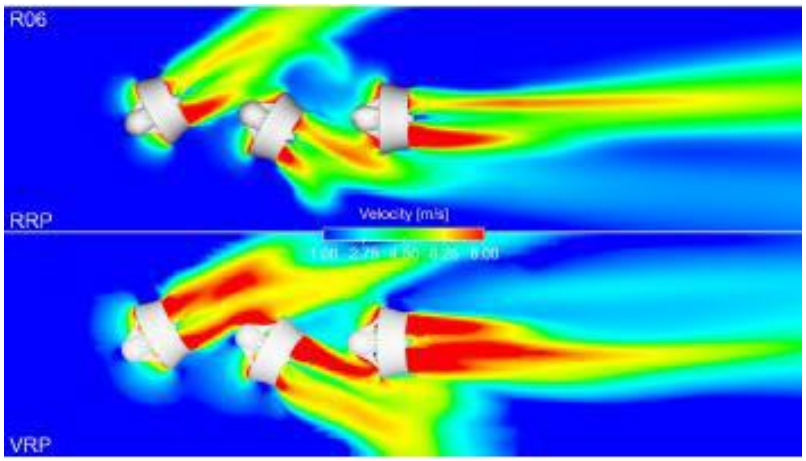

Source: Palm, Jürgens, and Bendl (2010) (Voith Turbo Marine).

This interaction is typically avoided by defining forbidden zones for some azimuth angles, where severe interaction occurs. Figure 2. 7 presents an example of a forbidden zone definition in order to avoid interactions between the azimuth thruster centrally placed and two other thrusters closely positioned. Note that the azimuth angle refers to the direction of the force it generates (the wake stream flows in the opposite direction).

Figure 2. 7 – Forbidden zone definition.

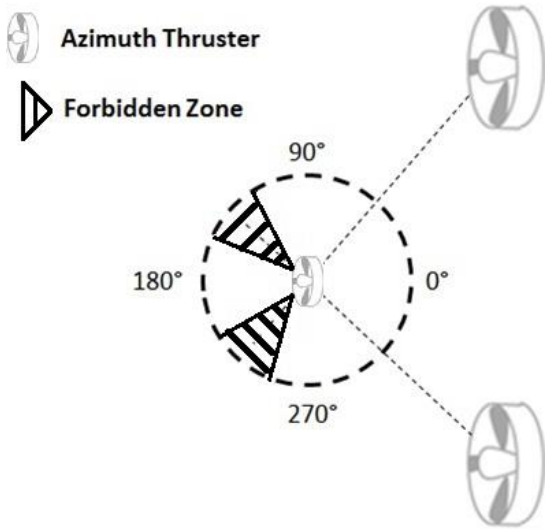

Source: Elaborated by the author.

2.6. Physical Limitations

In order to make the dynamic positioning system more reliable and accurate, some physical constraints of the thrusters should be considered.

2.6.1. Saturation

Saturation is the maximum thrust that a thruster can develop. It depends on the maximum rotation of the thruster and on its thrust coefficient. It is normally represented as a boundary with the following form:

$$|T| \leq T_{max} \tag{2.1}$$

Observe in Eq. 2.1 that the thruster can generate forces in two directions, by rotating its blades forward or backwards. In general, for azimuth thrusters the backward direction is avoided because it is less efficient. Througout this project it is considered that azimuth thrusters operate only in the forward deirection, therefore the restriction will be the same with the exception of the absolute operand; meaning T instead of $|T|$.

2.6.2. Maximum Rate of Turn and Maximum Rate of RPM

The physical limitations refer to the maximum rate of turn of the azimuth angle and the maximum rate of change of RPM of the propeller. Physically it means that it takes a certain time for the thruster to rotate 360°, or to change its thrust from 0 to T_{max}. The mathematical representation of these physical limitations is presented in Figure 2. 8, where δT represents the limited range of thrust and $\delta\alpha$ stands for limited range of azimuth angle.

Figure 2. 8 – Representation of the physical limitations.

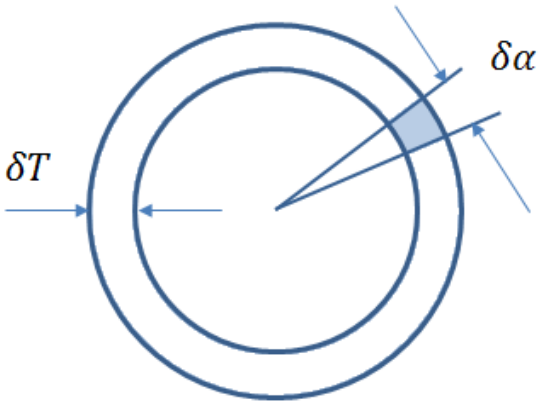

Source: Elaborated by the author.

3. THRUST ALLOCATION – STATE OF THE ART

In this section the evolution of the thrust allocation problem and the methods for solving it are presented. Moreover, some interesting recent developments are also presented and discussed.

3.1.1. Quadratic Power Function

This problem was the first step in the development of thrust allocation algorithms. The objective function Λ that represents the power consumed by the thrusters, is illustrated in Eq. 3.1 is a simplified to a quadratic function. This is an approximation of the real relation between the thrust and the power consumption. c_i represents the power constant and T_i is the thrust developed by each thruster.

$$\Lambda = P = \min_{T} \sum_{i=1}^{N} c_i \cdot {T_i}^2 \tag{3.1}$$

The constraints imposed to this problem are that the forces required by the control system (F_x, F_y, M_z), (not considering any hydrodynamic interaction) are matched by the forces generated by the thrusters. F_{x_i} and F_{y_i} are the forces developed by each thruster, x_i and y_i are the coordinates of the thrusters, respectively.

$$R: \begin{cases} \sum_{i=1}^{N} F_{x_i} - F_x = 0 \\ \sum_{i=1}^{N} F_{y_i} - F_y = 0 \\ \sum_{i=1}^{N} F_{y_i} \cdot (x_i) - \sum_{i=1}^{N} F_{x_i} \cdot (y_i) - M_z = 0 \end{cases} \tag{3.2}$$

The solution of this problem is quite simple and well known. The Lagrange multipliers method is used in order to obtain a linear system that is easily solved. When the thrusters are equal, it is possible to directly use the pseudo-inverse matrix

to solve this system. Some works as Wei *et al.* (2013) and Shi-Zhi *et al.* (2011a) used this method with good application in dynamic simulations.

Briefly, the Lagrange multipliers method joins the objective function and the constraints in one equation, by multiplying the constraints (R_i) by new variables (λ_i). This new function is called Lagrangean (L) and is represented in Eq. 3.3. This relaxes the problem since there are no more equality equations. The next step is to define the optimization condition, represented in Eq. 3.4, in which the Lagrangean gradient should be null (X are the design variables). If the solution obtained respects the KKT conditions ($\lambda_i \geq 0$), it is the point of minimal power consumption.

$$L = \Lambda - \lambda_i \cdot R_i \tag{3.3}$$

$$\frac{\partial L}{\partial X} = \frac{\partial L}{\partial \lambda} = 0 \tag{3.4}$$

3.1.2. Precise Power Function

The second step in the evolution of thrust allocation problems was to use the precise relationship between the developed thrust (T) and the power (P) required to generate it:

$$\Lambda = P = \min_{T} \sum_{i=1}^{N} c_i \cdot T_i^{\frac{3}{2}} \tag{3.5}$$

Note that this relationship is valid for conditions in which the vessel is in a stationary condition, known as bollard pull.

The constraints are the same as those shown in Eq. 3.2

This problem is also well known and has two efficient solutions:

1. Approximate the power by a quadratic equation (Eq. 3.6), and solve this problem as described in section 3.1.1.

$$P = a_0 + a_1 \cdot T + a_2 \cdot T^2 \tag{3.6}$$

2. Use Newton-Raphson method. The Newton method, shown in Figure 3. 1 is applied to the Lagrangean gradient (Eq. 3.4), because in order to obtain a minimum point, the Lagrangean gradient must be null. This approach is demonstrated in Van Daalen *et al.* (2011). Superficially, Newton-Raphson method consists of: at each iteration a step is taken in the opposite direction to the function gradient, until the gradient is null or until a stop criterion is reached.

Figure 3. 1 – Newton-Raphson Method.

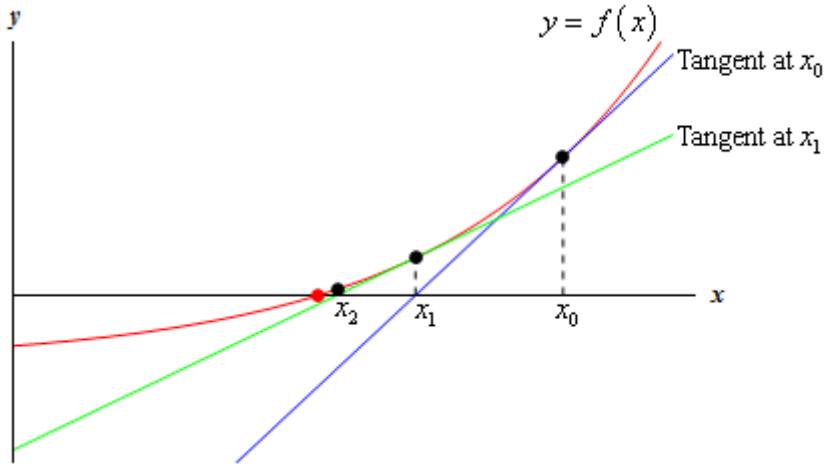

Source: Elaborated by the author.

3.1.3. Thruster Saturation

Including the thruster saturation ($T \leq T_{max}$) to the problem was the following the step. Observe that this is an inequality constraint. The first difficulty in solving the problem with this constraint is that it can be active or inactive. The second difficulty is that it may not be possible to solve the problem, in order words, once the thrusters are limited, it may be impossible to generate the forces required by the control system.

There are two solutions to deal with the saturation problem:

1. A conventional solution to this saturation problem is post-processing. Initially the problem is solved without considering the thruster limits (according to one of the methods presented in the last section). It is evaluated if one or more

thrusters should generate a thrust higher than its saturation. If this occurs, it is defined that this thruster will develop its maximum thrust in the azimuth angle of the current solution. Then a new thrust allocation is performed, considering the saturated thrusters as part of the external forces. This method can be seen in Arditti *et al.* (2015) and Van Daalen *et al.* (2011).

2. Another solution that was proposed to deal with the saturation is the relaxation of the problem (Arditti *et al.* 2014). By transporting the equality constraints to the objective function (Λ), a relaxed thrust allocation problem is obtained, as presented in Eq. 3.7. Weights (w_i) are defined in order to guarantee prioritization in the objective function towards the correct generation of the required forces, since it is a multi-objective function (minimization of power and generation of required forces).

$$\Lambda = \sum_{i=1}^{N} c_i \cdot T_i^{\frac{3}{2}} + \sum_{i=1}^{3} w_i \cdot {R_i}^2$$
$$T \leq T_{max} \tag{3.7}$$

Observe that the relaxed problem presented in Eq. 3.7 will not present any inconsistencies in case it is not possible to generate the required forces. It will minimize the error. Furthermore, it is possible to define a priority direction for force generation (surge, sway or yaw). Usually the prioritized direction is yaw, which prevents the vessel from rotating, since the rotation will probably increase the environmental forces over the vessel, as it usually operates in weathervane heading (the heading with the lowest environmental forces).

A method for solving the optimization problem in Eq. 3.7 is the Steepest-Descent (SD) method, represented in Figure 3. 2. The SD method is an iterative method that at each iteration gives a step of length γ in the opposite direction of the gradient of the objective function ($\overrightarrow{\nabla \Lambda}$).

Figure 3. 2 – SD Method.

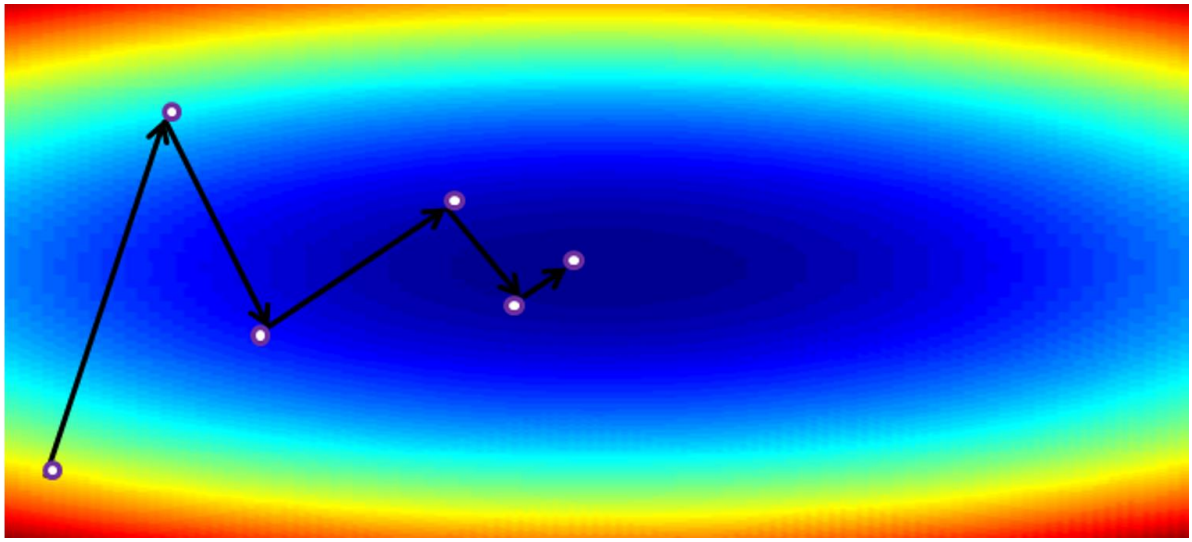

Source: Elaborated by the author.

3.1.4. Forbidden Zones (FZ)

A strategy to avoid hydrodynamic interaction between thrusters is the definition of forbidden zones. Figure 2. 7 presented this tactic. Eq. 3.8 presents the math representation of 20° around the forbidden angle $\alpha_{forbidden}$.

$$I: \left\{\left(\alpha_i - \alpha_{i_{forbidden}}\right)^2 \geq (10°)^2 \right. \tag{3.8}$$

There are two solutions to deal with the FZ problem, which are similar to the methods to deal with saturation. That is expected since both are inequality constraints.

1. Post-processing. In this case if the azimuth angle of one thruster is allocated inside its forbidden zone, it is set to the azimuth angle closer to the boundary. Then a new thrust allocation is performed, considering the azimuth angle of the referred thruster in the boundary of the FZ.
2. The second solution is working with the relaxed problem in Eq. 3.7 adding the FZ condition (Eq. 3.8). In this case the solution is applying the SD algorithm, making sure that at each step, the azimuth angles stay out of the FZ.

3.1.5. Inclusion of Main Propeller and Rudder

Recent studies suggest incorporating the main propeller and rudder to the DP System, which would increase the vessel maneuverability (De Wit 2009). Observe that the couple main propeller and rudder is able to generate forces in the sway direction when the force is forward and by positioning the rudder in the desired angle, as shown in Figure 3. 3.

Figure 3. 3 – Main Propeller and Rudder force generation capacity.

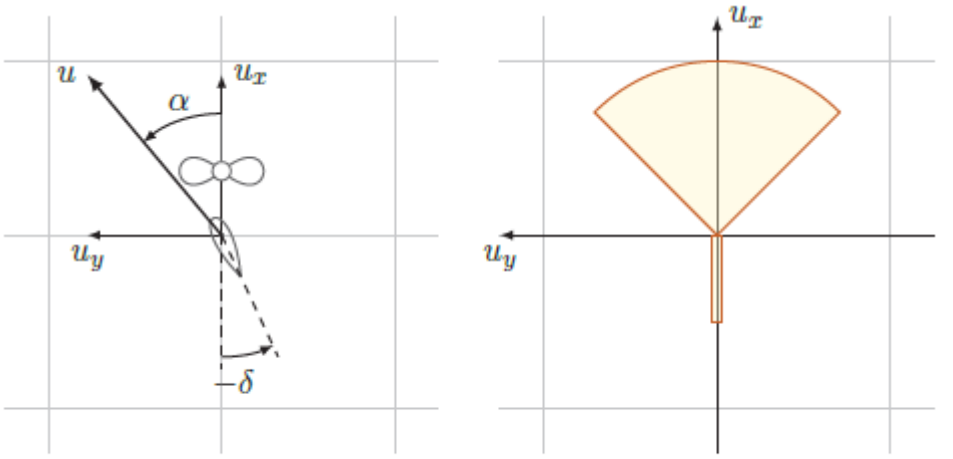

(e) Main propeller & rudder model. (f) Schematic thrust region for a propeller/rudder pair.

Source: De Wit (2009).

It is also worth mentioning the work of Granja, Madureira and Tannuri (2010), which performed numerical and model simulations of the station keeping of a vessel, using its main propeller and rudder.

3.1.6. Approximation of the viable space by a set of linear equations

Another interesting discussing presented in De Wit (2009) is the possibility of working with Cartesian coordinates by approximating the polar workspace of azimuth thrusters by a set of linear inequality constraints, as illustrated in Figure 3. 4. On the left side of the figure a circle is approximated by several line segments; on the right

side the result internal space, defined by the inequality constraints imposed to the blue line segments.

Note that the thrust allocation problem can be easily represented in Cartesian coordinates, with the exception of the saturation of the azimuth thruster. Therefore, with the approximation described, it is possible to work efficiently in Cartesian coordinates and to simplify the thrust allocation problem.

Figure 3. 4 – Approximation of circular thrust availability shape by linear inequalities.

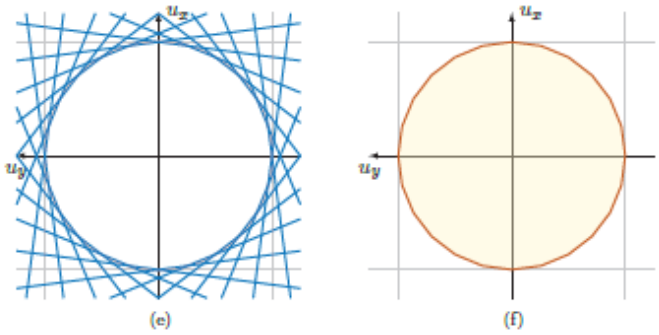

Source: De Wit (2009).

Although the approximation of the thrust region by linear inequalities provides an efficient method for dealing with circular thrust regions, it is not efficient when the thrust region is non convex, e.g. the thrust region of the couple main propeller and rudder presented in Figure 3. 3. The math definition of a convex viable space is presented in Eq. 3.9, where $Hess(g_i)$ represents the Hessian of the constraint, however the following geometrical interpretation is simpler to understand: If a viable space is convex, two points within the viable space can be united by a line segment, and all the points of this line segment are inside the viable space.

$$Hess(g_i) \leq 0 \tag{3.9}$$

The solution adopted in De Wit (2009) is to divide the thrust region is different convex viable spaces and solve a sub optimization problem for each combination of convex viable spaces. For example, the thrust region of the couple main propeller and rudder can be divided in two convex viable spaces. Observe that it increases the

computational time required for solving the thrust allocation problem, since the number of optimization problems increase exponentially with the number of convex viable space combinations.

Therefore, this solution is only efficient if it is not necessary to split the problem in various sub problems, which is in general true when the hydrodynamic interaction effects are not considered. However, when considering the thruster-hull and thruster-thruster effects on the thrust region, as shown in Figure 3. 5 it is easy to conclude that the division of the workspace in convex subspaces is not efficient, considering the amount of sub optimization problems.

Figure 3. 5 – Thrust region of an azimuth thruster considering hydrodynamic interaction effects.

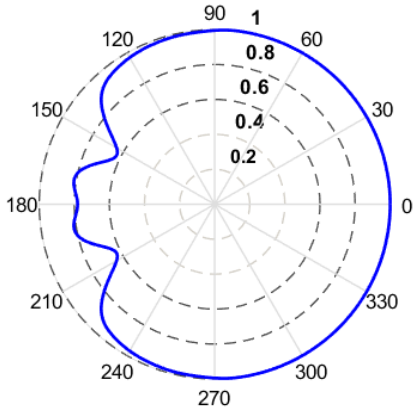

Source: Arditti, Cozijn and Van Daalen (2014).

3.1.7. Inclusion of Thruster Physical Limitation

The following step towards the evolution of thrust allocation algorithms was the inclusion of the thruster physical limitations. Johansen, Fossen and Berge (2004) present a solution for the inclusion of the rate of turn of azimuth thruster, by means of the Eq. 3.10 where α_0 is the current azimuth angle of the thrusters, $\dot{\alpha}_{max}$ is the maximum rate of turn of the azimuth angle and Δt is the time interval of each time step of the time domain simulation.

$$\Delta\alpha_{max} = \dot{\alpha}_{max} \cdot \Delta t$$
$$\alpha_0 - \Delta\alpha_{max} \leq \alpha \leq \alpha_0 + \Delta\alpha_{max} \tag{3.10}$$

In this work the authors also try to minimize the variation of the azimuth angle of the azimuth thrusters by including the term presented in Eq. 3.11 in the objective function (Ω is a weight matrix). Observe that by minimizing the variation of the azimuth angle, the wear and tear of the servomechanism responsible for the positioning of the thruster is minimized.

$$(\alpha - \alpha_0)^T \Omega (\alpha - \alpha_0) \tag{3.11}$$

By including the physical limitations (saturation and maximum rate of azimuth angle) it is possible that the thrusters cannot generate the required forces. The solution adopted is to relax the problem by means of slack variables (s), which appear both in the constraints and objective function, as demonstrated in Eq. 3.12 (Q is also a weight matrix).

$$\Lambda = \min_{T,\alpha,s} \left\{ \sum T_i^{1,5} + (\alpha - \alpha_0)^T \Omega (\alpha - \alpha_0) + s^T Q s \right\}$$
$$R: \begin{cases} \sum_{i=1}^{N} F_{x_i} - F_x + s_1 = 0 \\ \sum_{i=1}^{N} F_{y_i} - F_y + s_2 = 0 \\ \sum_{i=1}^{N} F_{y_i} \cdot (x_i) - \sum_{i=1}^{N} F_{x_i} \cdot (y_i) - M_z + s_3 = 0 \end{cases} \tag{3.12}$$

The method used in Johansen, Fossen and Berge (2004) to solve the thrust allocation problem was the SQP. Briefly, the SQP method (Nocedal and Wright 2002) consists in:

1) Locally approximating a complex problem.
    a. The nonlinear equalities are approximated by a set of linear equations (R_L). Observe that in this case a linear matrix L that depends on T_i and α_i will be equal to a linear independent vector b.

$$R_L: L(T_i, \alpha_i) = b \tag{3.13}$$

b. The objective function is approximated by a quadratic function, where a_i are constant matrix and $\mathbf{T}$ is the thrust vector.

i. $$\Lambda_Q = \mathbf{T} a_1 \mathbf{T}^T + a_2 \mathbf{T}^T + a_3 \tag{3.14}$$

2) Solving the local Quadratic Programming (QP) problem:

$$\begin{gathered} \Lambda_Q = \mathbf{T} a_1 \mathbf{T}^T + a_2 \mathbf{T}^T + a_3 \\ R_L: L(T_i, \alpha_i) = b \\ I: \{T_i \leq T_{max_i} \end{gathered} \tag{3.15}$$

3) From the new solution, repeating the steps above, using a convergence factor to stop the process.

QP refers to a class of optimization problems that have quadratic objective function and linear constraints. Many solutions have already been developed to this class of problems. Therefore, approximating the thrust allocation problem by a quadratic optimization is very efficient.

3.1.8. Avoiding Singularities

Johansen, Fossen and Berge (2004) present the concept of singularity. In order to explain this concept it is important to initially present the thrust matrix ($\mathbf{A}$), represented in Eq. 3.16, where α is the azimuth angle of the thrusters, x and y are the thruster coordinates. Note that by multiplying matrix $\mathbf{A}$ by the thrust vector $\mathbf{T}$, the forces generated by the vessel are obtained ($\mathbf{AT} = \mathbf{F}$).

$$\mathbf{A} = \begin{bmatrix} \cos(\alpha_1) & \cos(\alpha_2) & \dots \\ \sin(\alpha_1) & \sin(\alpha_2) & \dots \\ -y_1 \cos(\alpha_1) + x_1 \sin(\alpha_1) & -y_2 \cos(\alpha_2) + x_2 \sin(\alpha_2) & \cdots \end{bmatrix} \tag{3.16}$$

Matrix $\mathbf{A}$ only depends on the azimuth angle of the thrusters. In case they are positioned in a way that it is not possible to generate forces in one of the directions

(Surge, Sway and Yaw), matrix $\mathbf{A}$ is called singular. If $\mathbf{A}$ is singular, then the condition presented in Eq. 3.17 is true.

$$\det(\mathbf{A}\mathbf{A}^T) = 0 \tag{3.17}$$

In order to avoid this condition a new term is added to the objective function, as shown in Eq. 3.18. q is a weight constant, ϵ is a constant in order to avoid infinite values in case $\mathbf{A}$ is singular. Observe that by minimizing the term in Eq. 3.18, the term in Eq. 3.17 is maximized, avoiding singular conditions for matrix $\mathbf{A}$.

$$\frac{q}{\epsilon + \det(\mathbf{A}\mathbf{A}^T)} \tag{3.18}$$

The avoidance of singular conditions can be explained by the following example: If the control system does not require forces in all three directions (e.g. only surge), it is likely that all the thrusters are aligned with the surge axis. In that condition, if a sudden change in the external forces requires the generation of lateral forces, the vessel will not be able to generate them immediately due to the limited rate of azimuth angle, which will move the vessel away from its set-point.

The following sections present the most recent developments in thrust allocation.

3.1.9. Dynamic Definition of Forbidden Zones (FZ)

Xu, Wang and Wang (2016) present a dynamic definition of FZ. The size of the FZ is defined by the rotation speed ratio of two nearby thrusters. Figure 3. 6 presents the relation between the size of the FZ in degrees and the rotation ratio between the forward thruster (n_f) and the aft thruster (n_a).

Figure 3. 6 – Relation between the size of the FZ and the ratio between the rotation speeds of thrusters.

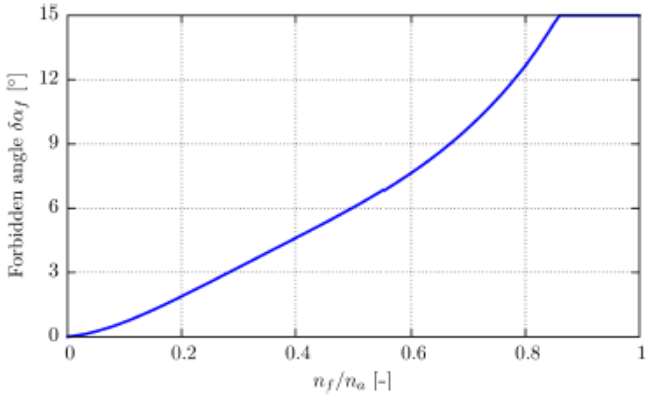

Source: Xu, Wang and Wang (2016).

By dynamically defining the size of the FZ it is possible to design a strategy to skip the FZ when its size is smaller than a predefined value (e.g. 5°). Therefore, the thruster-thruster interaction is minimized. In this work the interaction between thrusters is only considered by means of the effect on the inflow of the aft thruster (through the 4 quadrant diagram, Figure 2. 5).

It is an interesting approach since it guarantees that when the forward thruster directs its water jet over the aft thrust, the hydrodynamic effects are minimized. One disadvantage of this method is that it is necessary to define an external logic to define the best moment to skip the forbidden zone, and it may be possible that the forward thrust stays on the edge on both sides, crossing back and forward the FZ, increasing the wear and tear of the referred thruster.

3.1.10. Thrust Biasing

An approach for thrust biasing in presented in Wen, Xu and Fen (2016). Initially it is interesting to present the concept of thrust biasing illustrated in Figure 3. 7 – on the left no bias is applied; on the right a bias of 2 N is applied. It is a strategy in which two nearby thrusters generate the required forces by producing forces against each other (in a way the water jet of both of the thrusters does not interact with the other).

Figure 3. 7 – Thrust Biasing.

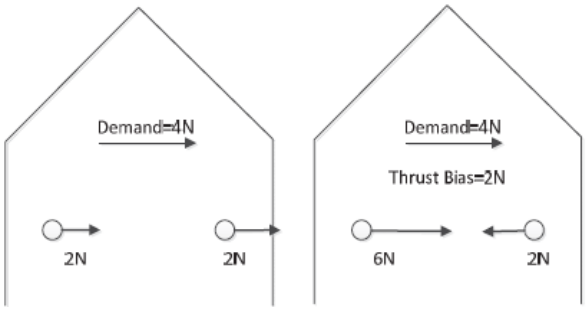

Source: Wen, Xu and Fen (2016).

Adopting this strategy has the following advantages:

1. Guarantees that thruster-thruster interaction does not happen between two nearby thrusters.
2. It can guarantee that the minimum thrust required for the operation of a thruster is used.
3. The response time to a sudden change in the environmental force is small, because this strategy automatically avoid singularities of $\det(\mathbf{A}\mathbf{A}^T)$.

This approach makes sense for relatively low environmental forces, where the thrusters are far from their saturation. In conditions where higher thrust generation is required it prevents the vessel from reaching its maximum capacity to withstand external loads.

Although thrust biasing is a well-known technique for generating the minimum thrust required for the operation of one thruster, the innovation presented in the work of Wen, Xu and Fen (2016) is a new definition of the couple of thrusters on bias according to the direction of the external forces. In this coupling technique, if the external forces are higher in surge direction than in sway direction, the thrusters aligned in the surge axis of the vessel are coupled. If the sway forces are dominant, the thrusters aligned in the sway direction are coupled.

3.1.11. Minimization of Power Variation

The work by Ding, Yang and Huang (2016) suggests the inclusion of a new term in the objective function in order to minimize the power variation (Eq. 3.19). *O* is a weight constant.

$$\Delta P \cdot O \cdot \Delta P^T = \left(\sum c_i {T_i}^{1,5} - c_i {T_{i_0}}^{1,5}\right) O \left(\sum c_i {T_i}^{1,5} - c_i {T_{i_0}}^{1,5}\right)^T \quad (3.19)$$

The stabilization of power consumption helps to stabilize the power grid of the vessel.

3.1.12. Modulation of the Vessel Electric Bus through Thrust Allocation

Veksler *et al.* (2015) present a thrust allocation algorithm taking into account the electric bus demands of the vessel. Note that the force generation system consumes more than 50% of the power generated in the vessel; therefore, it is important to minimize the impacts of high load variations in the electric bus and frequency of the network.

The algorithm makes sure that thrust allocation responds according to the vessel needs of power.

- In case the vessel needs to spend more power the solution is through thrust biasing.
- In case the vessel requires more power, since the thrust allocation is already optimized, the solution is to allow a small deviation from the set point, in order to return shortly.

In order to achieve this functionality, the dynamic system of the vessel is considered. The objective function gains new terms in order to represent the power variation and the minimization of position and velocity errors. Also, new inequality constraints are added to limit the maximum error in position and speed.

Adding these terms to the problem make it significantly more complex, since the error in position and speed depend on the vessel dynamic model. The difficulties in working with such a complex optimization problem are:

- Defining the best weights for the multi-objective function.
- The time consumption required for solving a complex optimization problem, with the need to model the dynamic of the vessel at each iteration.

Nevertheless, the results presented in the paper are interesting and can lead to new improvements in the DP system.

3.1.13. Model Predictive Control (MPC)

Veksler et al. (2016) presents the concept of MPC for thrust allocation. Figure 3. 8 illustrates the concept. On the left, the usual feedback control system is presented with a higher-level control for vessel dynamics (definition of required forces), a medium level thrust allocation algorithm and low level thruster control. On the right, the MPC that incorporates the thrust allocation algorithm to the high level dynamic control.

Figure 3. 8 – Usual feedback control system vs MPC.

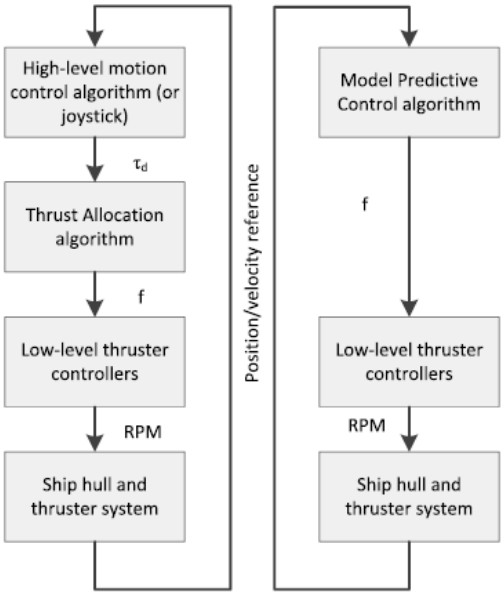

Source: Veksler *et al.* (2016).

In this work the dynamic model of the vessel is incorporated into the objective function and constraints, which configures the MPC characteristics. Specifically in this project the objective is that the vessel follows a pre-defined route with a maximum deviation, minimizing the power consumption.

The simulation results presented in Veksler *et al.* (2016) show a significant gain in the power consumption by incorporating the power optimization (thrust allocation) to the high level dynamic control. It can be understand as: In the MPC the thrust allocation is optimized throughout the entire trajectory, with predictive information of all the time steps as one single optimization, whereas the usual DP system optimizes each time step of the trajectory discretely.

3.1.14. Probabilistic Thrust Allocation Algorithms

Recent implementations of probabilistic optimization methods were applied to solve the thrust allocation algorithms. Mauro and Nabergoj (2016) suggest the use of a genetic optimization method. Wu, Ren and Zhang (2016) solve the thrust allocation

algorithm by means of an algorithm based on the behavior of a bee colony. And Ding, Yang and Huang (2016) use a method based on the behavior of a fish swarm.

Figure 3. 9 presents behavior of a genetic algorithm. It is a simplified example of the selection of the best point for one azimuth thruster, limited only by saturation:

1. Initially a random distribution of points is generated (parents – 1st generation).
2. The parents give birth to children that are random combinations of the parents (children – 1st generation).
3. The best from the 1st generation (parents and children) become the parents of the second generation.
4. The parents from the 2nd generation give birth to the children of the 2nd generation.
5. This process continues until the algorithm converges to the best point.

Figure 3. 9 – Genetic algorithm

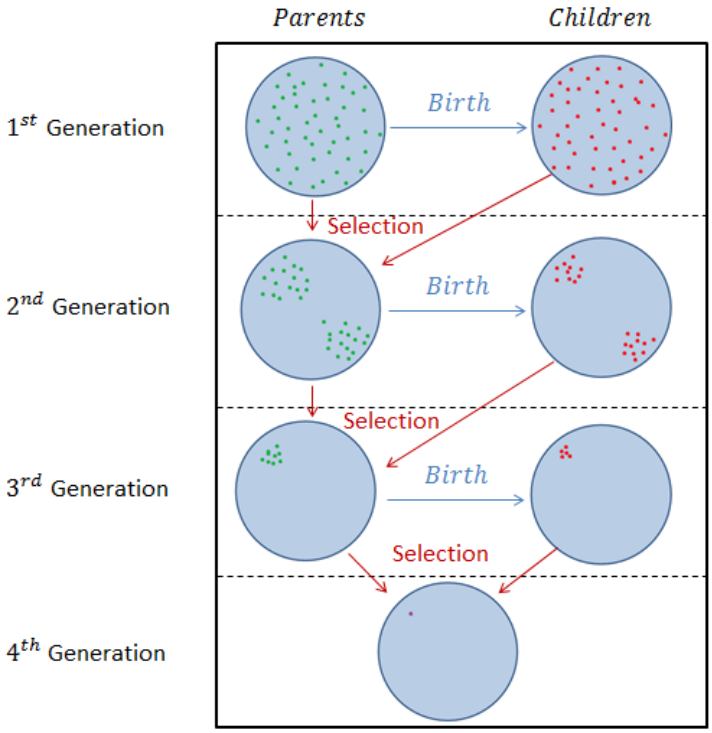

Source: Elaborated by the author.

Note that the behavior of the genetic algorithm can be seen as the survival of the fittest (as in the evolution of species). The bee colony and fish swarm algorithms simulate the behavior of these animals in search for food.

In general, the application of probabilistic algorithms is simple, since only the objective function information is used to evaluate the solutions and it is verified if the candidates respect the restrictions. These algorithms are similar to a global search, in which the favorable sites are observed in more detail.

The probabilistic algorithms claim they can find the global minimum more efficiently because they do not get stuck in local minima, like numerical methods.

The disadvantage of probabilistic algorithms is that they are slow due to elevated number of evaluations and generation of new candidates. Therefore, these algorithms are not ideal for real time applications nor fast time simulations.

4. MODELLING THE OPTIMIZATION PROBLEM

In this section the effects of the hydrodynamic interaction effects are presented: thruster-hull, thruster-current and thruster-thruster. Once different methods for representing each interaction separately are explained, a structured model is defined in order to consider all the hydrodynamic interaction effects together, including a novel model for thruster-thruster interaction.

The effects of the hydrodynamic interaction effects on the thrust allocation problem are detailed, observing that the interactions affect both the thrust generation and the required power.

The couple main propeller and rudder is also characterized. It can be represented as a modified azimuth thruster, since two variables are controlled (thrust and rudder angle).

Finally, the physical limitations are modeled in accordance with the structure of an optimization problem.

The result of the efforts in this chapter is the thrust allocation problem represented as an optimization problem, with all the hydrodynamic interactions and physical limitations mathematically modelled.

4.1. Hydrodynamic Interaction Effects

4.1.1. Thruster-hull

There are mainly three methods for representing the thruster-hull interactions. The first one is an analytic method described in the ABS GUIDE FOR DYNAMIC POSITIONING SYSTEMS (ABS 2013). The second one is through CFD calculation, which compared with Particle Image Velocimetry (PIV) measurements provided interesting insight on thruster-hull interactions, as described in Cozijn and Hallmann (2013). The third method is obtaining the data by means of model testes (Arditti and Tannuri 2012).

ABS GUIDE FOR DYNAMIC POSITIONING SYSTEMS

The ABS GUIDE FOR DYNAMIC POSITIONING SYSTEMS (ABS 2013) provides analytical equations for considering the thruster-hull interaction for ships. The thrust degradation due to hull friction is related to the length (L) and breath (B) of the hull. Figure 4. 1 presents the reduction ratio due to hull friction.

Figure 4. 1 – Thrust reduction due to friction on the hull.

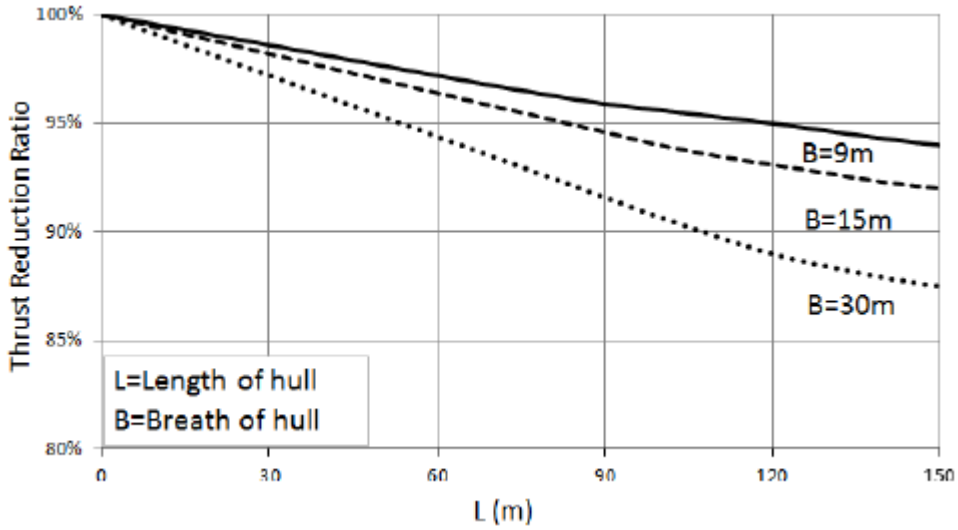

Source: ABS (2013).

The Coanda effect is related to the bilge radius and the length of the flow underneath the hull. According to ABS (2013) if no detailed data is available, the thrust reduction ratio caused by the Coanda effect can be taken as 97%.

The blockage of the wake flow by a platform pontoon occurs when one thruster directs its water jet towards a pontoon. The reduction of the net thrust due to pontoon blockage can be calculated according to Eq. 4.1, where η_p is the efficiency (thrust reduction ratio) due to pontoon blockage, L_p is the length of the downstream centerline between the thruster and the pontoon and $K_p = 1$ (schematic representation in Figure 4. 2).

$$\eta_p = 0.8K_p \frac{L_p}{55} \tag{4.1}$$

Figure 4. 2 – Schematic representation of downstream length.

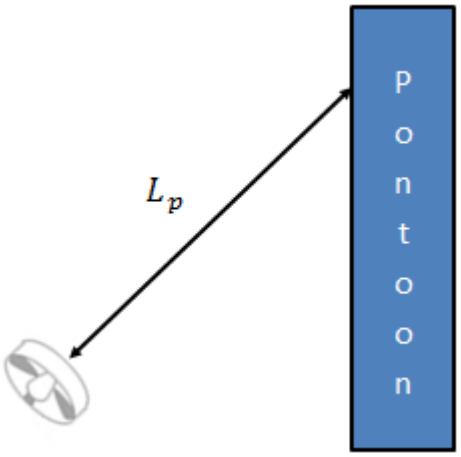

Source: Elaborated by the author.

CFD

It is possible to study the thruster hull interactions by means of CFD calculations. In Cozijn and Hallmann (2013) the CFD calculations were compared with PIV measurements (represented in Figure 4. 3) with good results.

Figure 4. 3 – PIV measurements of the wake velocity field.

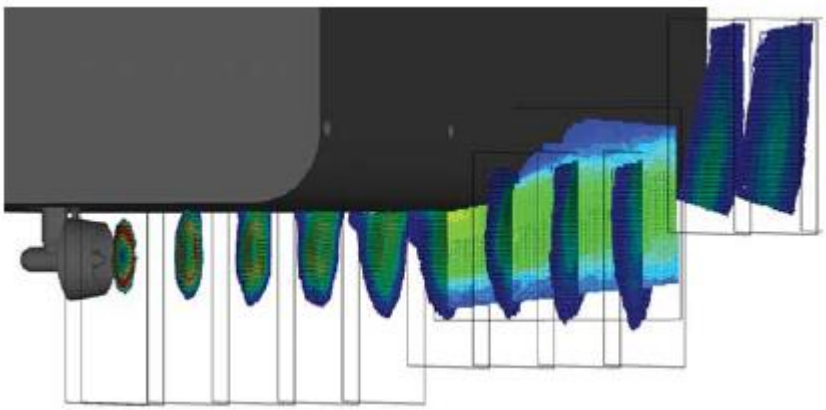

Source: Cozijn and Hallmann (2012).

The CFD technique allows the prediction of the wake flow speed and form with high precision (as demonstrated in Figure 4. 4). Once the wake velocity field is

estimated it is possible to calculate the efficiency loss of thrust generation due to thruster-hull interaction.

Figure 4. 4 – CFD study of the pontoon blockage of the wake flow of the thruster.

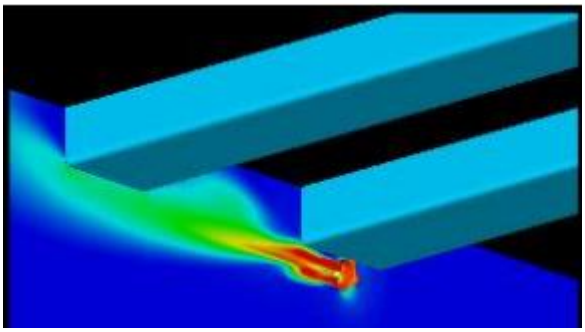

Source: Jurgens *et al.* (2008).

MODEL TESTS

A different approach to obtain the efficiency curves of the thrusters is through experiments with small scale vessel models. The term efficiency curve is used because azimuth thrusters can rotate 360°, and for every angle a different interaction occurs, therefore, the efficiency is defined for different operating angles. The experimental method used in Arditti and Tannuri (2012) was to measure the thrust generated in different azimuth angles ($T(\alpha)$) and compare it with the bollard pull thrust (T_B).

The thrust test conducted is shown in Figure 4. 5. This configuration using a load cell allows obtaining the forces generated in surge and sway directions, namely F_x and F_y. In this test each thruster is tested separately in different angles; the net forces measured by the load cell for each test point allow comparing the generated thrust with the thrust in bollard pull condition, which defines its efficiency for this angle.

Figure 4. 5 – Thrust test.

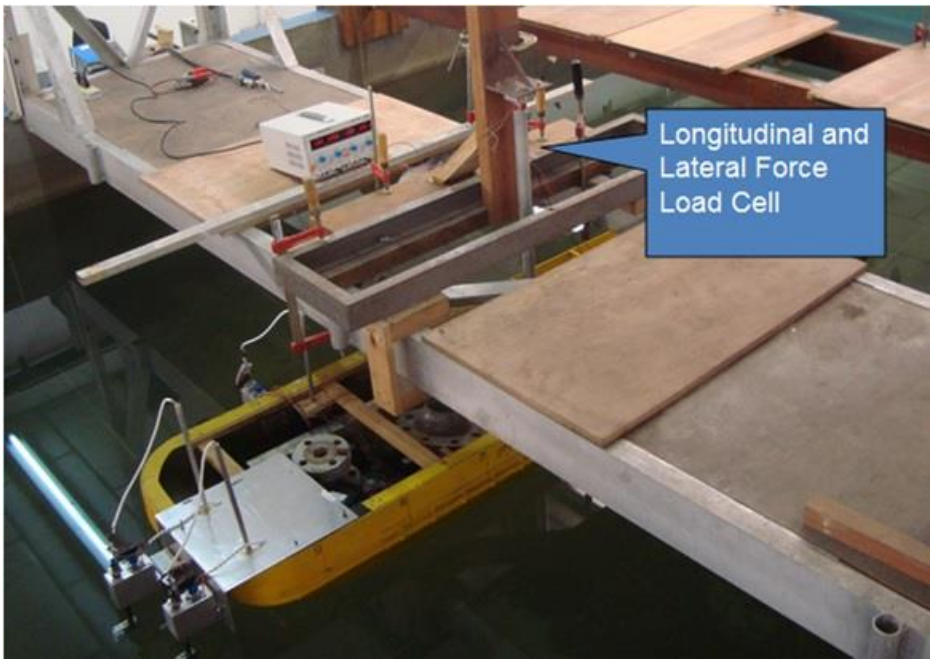

Source: Arditti and Tannuri (2012).

The efficiency curves obtained in the described thrust test are shown in Figure 4. 6. The form of the efficiency curves is related with the hydrodynamic interaction effects. Note that the curves are only valid for this vessel, for a different vessel with a different thruster configuration the efficiency curves will be different.

Comparing the results with the hypothesis for each interaction, it can be noticed that the method to determine the efficiency curves was qualitatively efficient. For example, thruster 6 has a reduced efficiency when the water jet interacts with the hull (from 150° to 240°) and when the water jet interacts with thruster 5 (around 120°). Therefore, the experimental method can represent different types of interference (between thrusters and thruster-hull). Furthermore, the polar coordinates representation for the efficiency curve is ideal to account for all the interaction phenomena.

Figure 4. 6 – Efficiency curve of the thrusters obtained by model tests.

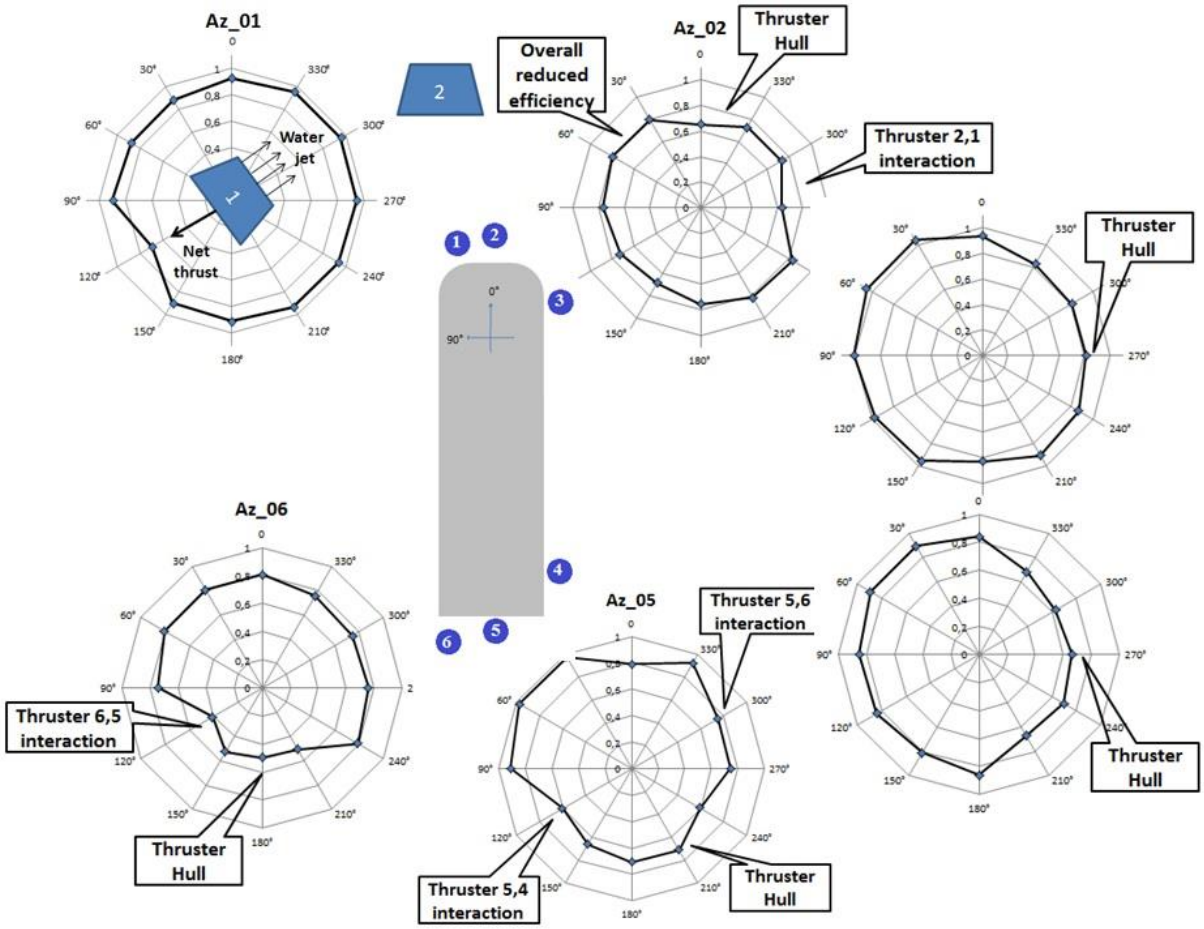

Source: Arditti and Tannuri (2012).

4.1.2. Thruster-current

There are mainly two methods for representing the thruster-current interactions. The first one is an analytic method described in the ABS GUIDE FOR DYNAMIC POSITIONING SYSTEMS (ABS 2013). The second method is using the 4 quadrant diagram.

ABS GUIDE FOR DYNAMIC POSITIONING SYSTEMS

The ABS GUIDE FOR DYNAMIC POSITIONING SYSTEMS (ABS 2013) provides analytical equations for considering the thruster-current interaction. The current inflow may reduce the net thrust of the thrusters. The thrust reduction can be calculated using the graph in Figure 4. 7.

Figure 4. 7 – Thruster-current interaction.

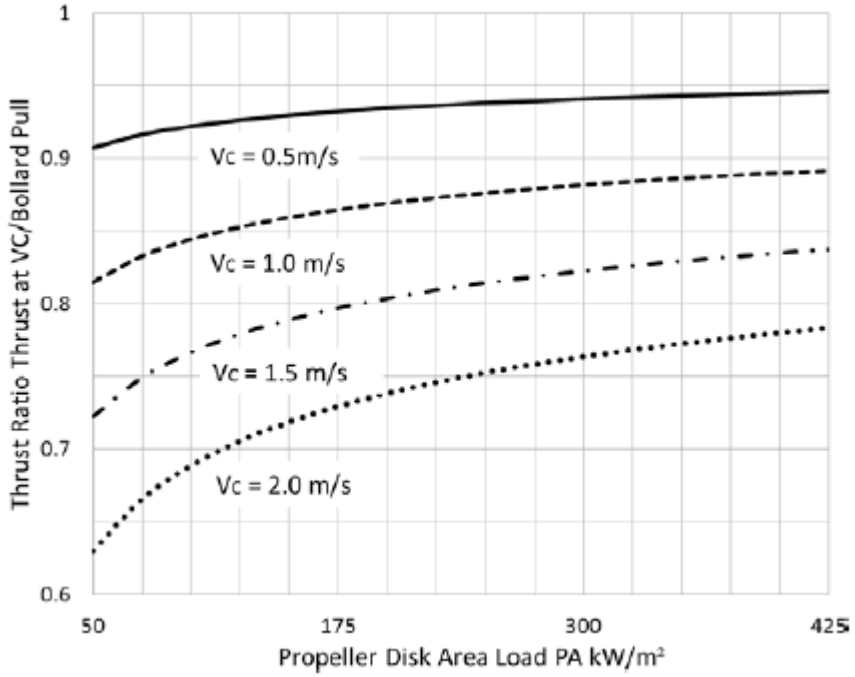

Source: ABS (2013).

The thruster efficiency loss can also be calculated according to Eq. 4.2, where η_c is the efficiency (thrust reduction) due to current inflow, V_{cur} is the current speed, PA is the propeller disk area load (the power consumed by the thrusters divided by its circular area - in kW/m^2) and $K_{c1} = 400$ and $K_{c2} = 0.11$. This formula is valid for currents up to $2m/s$.

$$\eta_c = 1 - \left(\frac{K_{c1}}{PA}\right)^{0.25} \cdot K_{c2} \cdot V_{cur} \tag{4.2}$$

4 QUADRANT DIAGRAM

The effects relative to thruster-current interaction can be modelled according to the knowledge of the hydrodynamic performance of the thruster. Figure 2. 5 presents the 4 quadrant diagram data of a thruster, that shows the thrust and torque coefficients (C_T and C_Q) for a wide range of operational points (including back and forward thrust, and current arriving from the front or from the back of the thruster).

Eq. 4.3 shows how C_T and C_Q affect the thrust and power (respectively), where ρ is the water density, n is the angular speed of the thruster and D is the diameter of the thruster.

$$T = C_T \cdot \rho \cdot n^2 \cdot D^4$$
$$P = C_Q \cdot \rho \cdot n^3 \cdot D^5 \quad (4.3)$$

The procedure for calculating β is presented in Eq. 4.4. J is the advance speed ratio, $V_{projected}$ is the projected current speed on the thruster, n is the thruster speed of rotation, D is the thruster diameter, μ_{cur} is the current attack angle and α is the thruster azimuth angle.

$$J = \frac{V_{projected}}{n \cdot D} = \frac{V \cdot |\cos(\mu_{cur} - \alpha)|}{n \cdot D}$$
$$\beta = \text{atan}\left[\frac{J}{0.7\pi}\right] \quad (4.4)$$

Figure 4. 8 – Schematic overview of the variables regarding the inflow current.

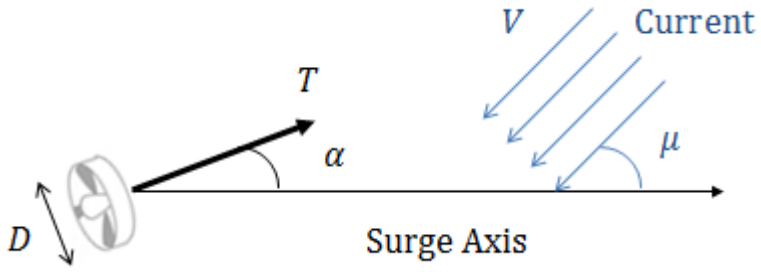

Source: Elaborated by the author.

Note that the thruster-current interaction affects the delivered thrust (C_T) and the required power (C_Q). Moreover, observe that when the thrust coefficient decreases, the torque coefficient also decreases (the opposite is also true). This relation can be easily explained by the following case: If the current is incoming at the thruster with some speed the blades cannot accelerate it as much as if it was still,

because the relative speed of the blades and the water is smaller (C_T decrease), on the other hand, the effort (power) to accelerate the current is smaller, since it already has an initial velocity (C_Q decrease).

4.1.3. Thruster-thruster

In order to estimate the thruster-thruster interaction there are two methods. The first one is available in the ABS GUIDE FOR DYNAMIC POSITIONING SYSTEMS (ABS 2013). The second method is using the 4 quadrant diagram.

ABS GUIDE FOR DYNAMIC POSITIONING SYSTEMS

The ABS GUIDE FOR DYNAMIC POSITIONING SYSTEMS (ABS 2013) provides analytical equations for considering the thruster-thruster interaction. Figure 4. 9 presents the thrusters configuration considered for the calculation of the hydrodynamic interaction. Observe that the distance between the thrusters and their diameter are important for the estimation of efficiency loss.

Figure 4. 9 – Configuration considered for thruster-thruster interaction.

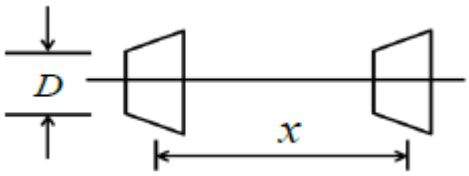

Source: ABS (2013).

Eq. 4.5 presents the efficiency of the downstream thruster due to interactions with the forward thruster. η_t is the efficiency of the downstream thruster due to thruster-thruster interaction, x is the distance between the thrusters and D is the diameter of the thrusters.

$$\eta_t = 1 - 0.75^{(x/D)^{\frac{2}{3}}} \quad (4.5)$$

Figure 4. 10 presents the efficiency loss due to thruster-thruster interaction for various cases of thruster diameter and distance ratio.

Figure 4. 10 – Thrust reduction of the downstream thruster in open water.

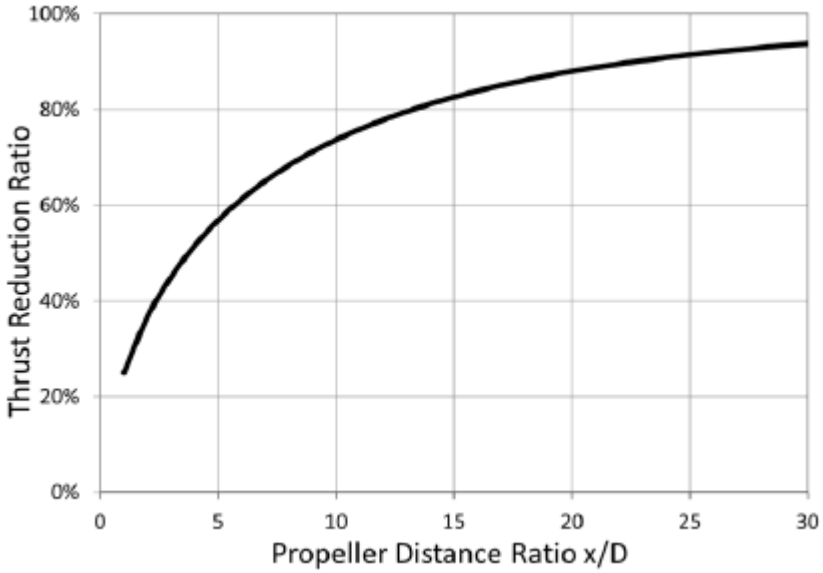

Source: ABS (2013).

Figure 4. 11 presents the configuration considered for estimating thruster-thruster interaction in case the upstream thruster is turning.

Figure 4. 11 – Thrusters configuration in tandem condition turning the upstream thruster.

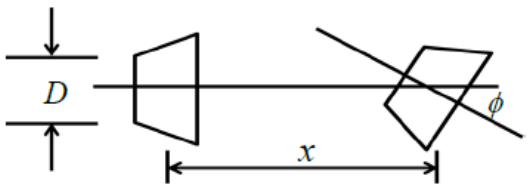

Source: ABS (2013).

Eq. 4.6 presents the formula for calculating the efficiency loss of the downstream thruster due to interactions with the forward thruster (when it is turning). $\eta_{t\varphi}$ is the efficiency of the downstream thruster due to thruster-thruster interaction, η_t is the thrust reduction ratio at zero steering angle, x is the distance between the thrusters, D is the diameter of the thrusters and φ is the relative angle between the forward thruster and the centerline that connects the thrusters.

$$\eta_{t\varphi} = \eta_t + (1 - \eta_t) \cdot \frac{\varphi^3}{\frac{130}{{\eta_t}^3} + \varphi^3} \tag{4.6}$$

Figure 4. 12 presents the efficiency loss due to thruster-thruster interaction for various cases of thruster diameter and distance ratio.

Figure 4. 12 - Thrust reduction of the downstream thruster considering steering angles of the upstream thruster.

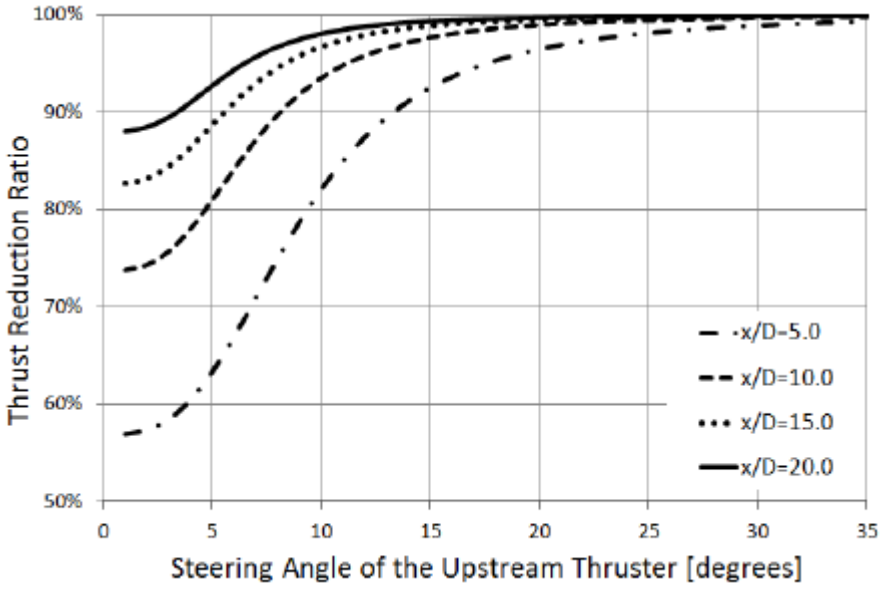

Source: ABS (2013).

The ABS guide also provides a method for calculating the range of the forbidden zones in order to avoid thruster-thruster interaction. Figure 4. 13 and Table 4. 1provide the range of the forbidden zone for various cases of thruster diameter and distance ratio.

Figure 4. 13 – Range of forbidden zone.

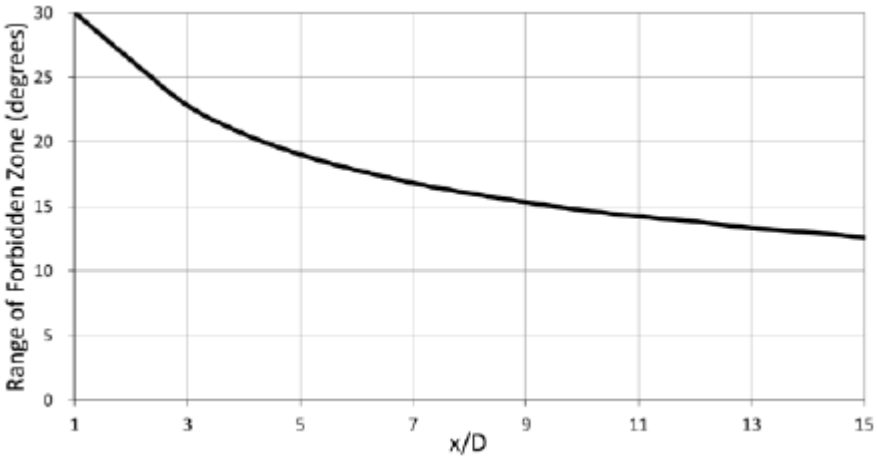

Source: ABS (2013).

Table 4. 1 – Range of forbidden zone for different x/D.

x/D	Angle [°]	x/D	Angle [°]	x/D	Angle [°]
1	30	6	17.8	11	14.2
2	26.3	7	16.8	12	13.8
3	22.8	8	16	13	13.3
4	20.6	9	15.3	14	13
5	19	10	14.7	15	12.6

4 QUADRANT DIAGRAM

It is also possible to calculate the thruster-thruster interaction effects by means of the 4-quadrant diagram (Figure 2. 5). In this case it is necessary to calculate the water flow generated by one thruster over the other. Observe that in this case the wake flow will act similarly to the natural current, therefore allowing the use of the calculations with the 4-quadrant diagram.

In this case additional effort is spent on calculating the wake flow at the exit of the thruster, and the respective induced current it generates in other thrusters. The method used for calculating the induced current is presented in the following section.

4.2. Combination of hydrodynamic interaction effects

The most important definition to be made is how to represent the interaction effects within the thrust allocation process. When considering only simple cases, such as thruster-hull interaction, it has been made with efficiency functions, more specifically polar plots of the efficiency (Arditti *et al.* 2015).

Since this solution works it would be straight forward to expand it to all the interaction effects considered (thruster-hull, thruster-thruster and thruster-current) and add the effects. However, the interaction effects are rather complicated, and one interaction effect can affect the other (e.g. thruster-current and thruster-thruster). Therefore, adding the different effects is not an acceptable solution.

Nevertheless, representing all the interaction effects to its details is impossible due to the complex nature of the physical phenomena and the combination of different interactions. Furthermore, it is not necessarily required to represent perfectly the interactions, because as more detailed as the representation gets, the more complicated the allocation problem becomes, and the more time consuming it is. Therefore, a compromise solution should be considered in order to represent as much as possible the interaction effects, without turning it into a problem with no solutions or extremely time consuming.

Regarding the loss of efficiency of one thruster alone, observe that it occurs due to effects of two natures: Inflow and Wake flow as represented in Figure 4. 14. The phenomena related to the inflow of the thruster (caused by natural and induced currents) define both C_T and C_Q, which provide the “state” of the thruster. The phenomena related with the wake flow of the thruster causes loss of efficiency because its water jet drags along the hull and cause pressure fields over an area of the vessel (e.g. pontoon, another thruster or subaquatic equipment).

Figure 4. 14 – Inflow and Wake flow phenomena.

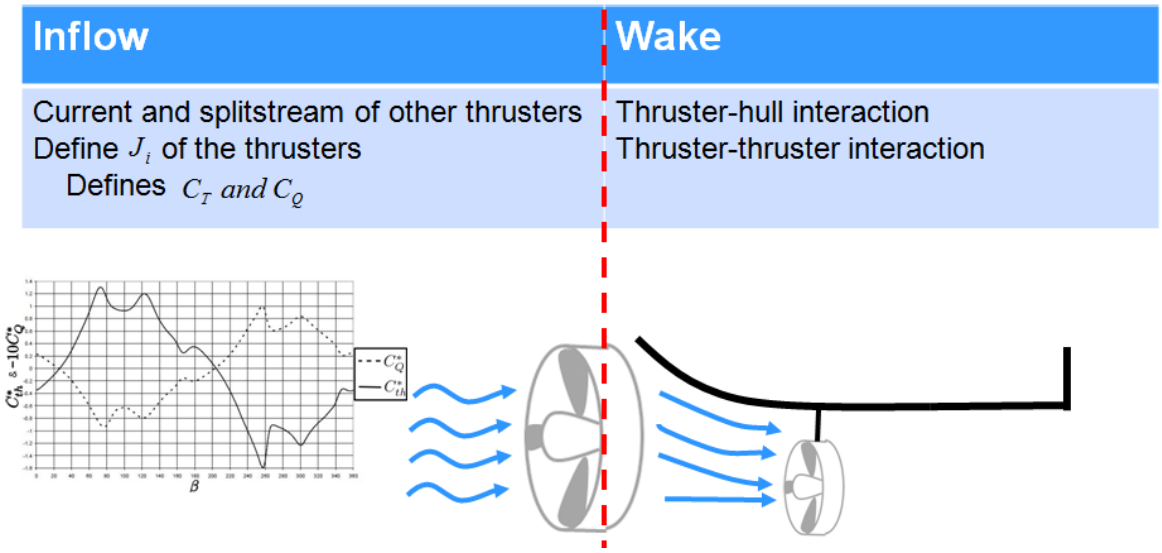

Source: Arditti, Cozijn and Van Daalen (2014).

The following sections present a method for calculating the effects of the inflow and wake flow phenomena. Observe that once the interactions are separated in this form, the effects can be added, because they occur independently (for each thruster alone).

4.2.1. Inflow

In order to calculate the effects of the inflow phenomena on a thruster, the 4 quadrant diagram is used. Observe that it is valid for both thruster-current and thruster-thruster interactions, which makes it a more powerful tool than the analytic functions defined in the ABS guide.

In order to determine the state of the thruster, C_T and C_Q are calculated according to Eq. 4.5 and the 4 quadrant diagram. The difference in this case is that the inflow current is the combination of the natural current and the induced current generated by the other thrusters. Therefore a model for the estimating the induced currents and its combination with the natural current are presented.

WAKE FLOW MODEL

In order to represent the wake flow of a thruster and calculate the current it generates, a model is defined to represent it. Figure 4. 15 shows the defined model, where the thruster generates a water jet that spreads within an area defined by the spread angle. The spread angle (θ) depends on the type of thruster, it can be obtained by means of CFD calculations or PIV experiments, as shown in Figure 4. 3. Furthermore, in this model it is possible to determine a fictional origin (O) for the wake flow.

Figure 4. 15 – Wake flow model with spread angle and origin.

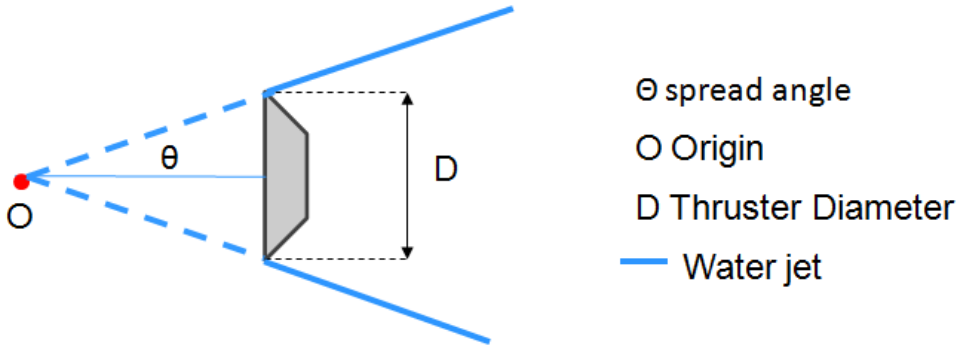

Source: Arditti, Cozijn and Van Daalen (2014).

The method for determining the fictional origin (O_i) of the wake flow is demonstrated in Figure 4. 16, where P is the position of the thruster, θ is the spread angle of the wake flow, D is the diameter of the thruster, and L is the distance between the thruster and its fictional origin (the formula for calculating L is also represented in the Figure).

Figure 4. 16 – Determining the fictional origin of the wake flow.

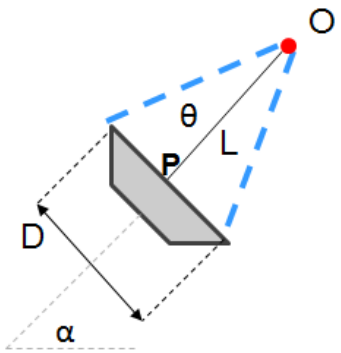

$$P = (x, y)$$

$$L = \frac{D}{2 \cdot tg(\theta)}$$

$$O_i = (x + L \cdot \cos\alpha, y + L \cdot \sin\alpha)$$

Source: Arditti, Cozijn and Van Daalen (2014).

CHECKING INTERACTION

Once the origin of the wake flow is determined, it is possible to check whether the wake flow of one thruster will affect another thruster. It is determined by evaluating if the angle that connects T_2 with T_1 ($Link_{2\rightarrow1}$) is within the direction of the water jet considering its spread angle ($-\alpha_2 \pm \theta_2$). If this verification is true, it means that the wake flow of T_2 causes an induced inflow current on T_1.

Figure 4. 17 – Method for checking thruster-thruster interaction.

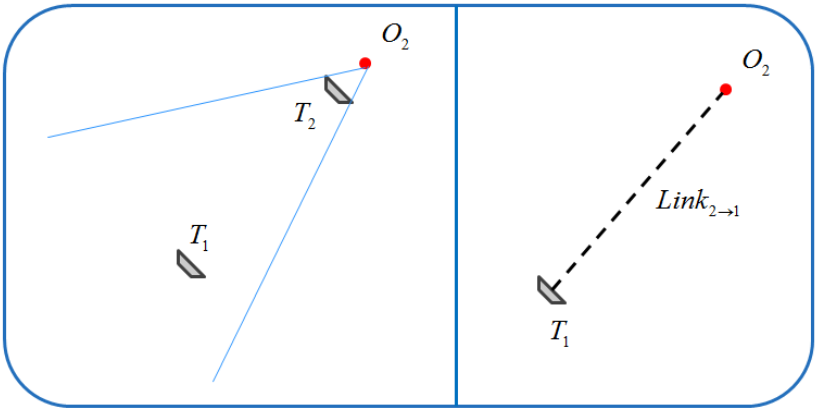

Source: Arditti, Cozijn and Van Daalen (2014).

FLOW MODEL

To determine the speed of the induced current, a flow conservation model with cargo loss dependent of the travelled distance (x) of the water jet is used. In Eq. 4.7

the flow in position x ($Q_f(x)$) depends of the cargo loss function f_{LL}, which is a linear function with respect to the Jetstream traveled distance (x) and *k* is a constant value. Observe that the average speed of the flow at the traveled distance x is easily found considering the area of the flow ($A(x)$), which depends on the spread angle (θ), as illustrated in Figure 4. 6. Furthermore, the current speed also depends on the radial distance of the interaction point (r) and the flow radial spread (R) with respect to the average speed of the flow ($v_{average}$), as represented in Eq. 4.8. This method is consistent with PIV measurements represented in Figure 4. 18.

$$Q_f(x) = Q_{f_0} \cdot f_{LL}(x) = Q_{f_0} \cdot \frac{k}{k+x}$$
$$v_{average}(x) = \frac{Q_f(x)}{A(x)} \tag{4.7}$$

$$v(r,x) = 2 \cdot v_{average}(x) \cdot \left(1 - \frac{r^2}{R(x)^2}\right) \tag{4.8}$$

Figure 4. 18 – Wake flow PIV measurements.

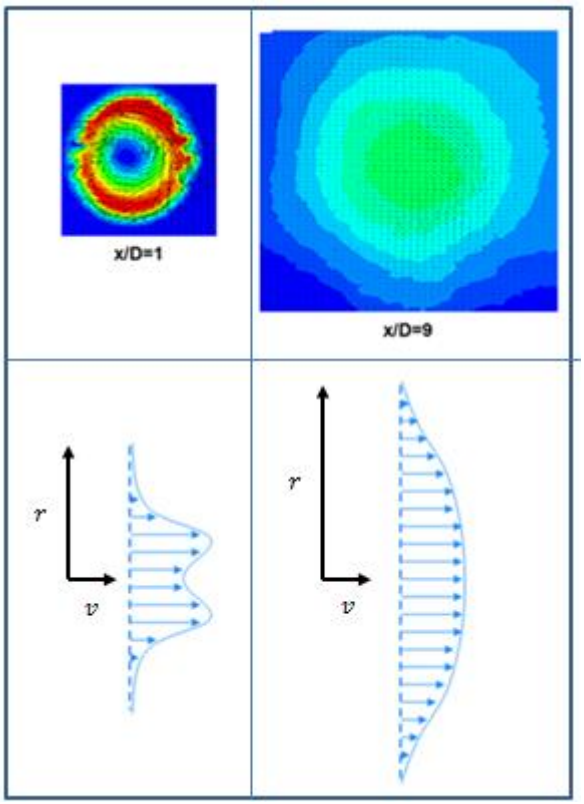

Source: Arditti, et al (2018).

WAKE FLOW SPEED AT THE EXIT OF THE THRUSTER

Once the model for calculating the induced current has been discussed, the formula for calculating the average speed of the wake flow in the exit of the thruster is presented in Eq. 4.9, where $V_{j_{exit}}$ is the average speed of the wake flow in the exit of the thruster, V_{Inflow} is the average speed of the inflow, T is the generated thrust, ρ is the water density and A is the circular area of the thruster.

$$V_{j_{exit}} = \sqrt[2]{V_{Inflow} + \frac{2 \cdot T}{\rho \cdot A}} \tag{4.9}$$

AVERAGE CURRENT VELOCITY NEAR OTHER THRUSTERS

Finally, to determine the travelled distance of the water jet (x) and the radial distance (r) at the interaction point, the trigonometric model presented in Figure 4. 19 is used, together with the following correspondent equations. Note that d and $\delta_{T2 \to T1}$ are the distance and the angle between the thrusters, respectively.

Figure 4. 19 – Trigonometric model of the Wake flow interaction.

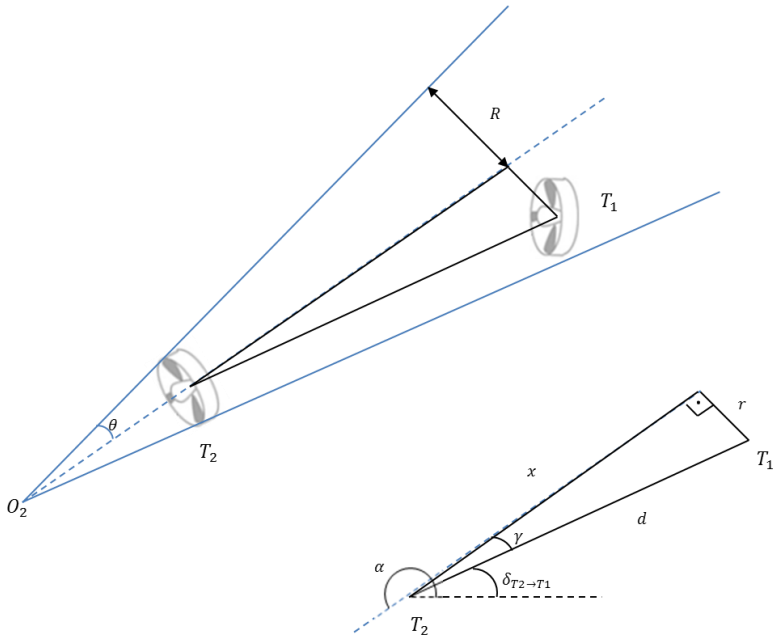

Source: Arditti, et al (2018).

$$\gamma = \alpha_2 - \pi - \delta_{T2 \to T1}$$
$$x = d \cdot \cos(\gamma) \tag{4.10}$$
$$r = d \cdot \sin(\gamma)$$

COMBINATION OF NATURAL CURRENT AND INDUCED CURRENTS

The result inflow in one thruster is calculated as the vector sum of the natural current and all induced currents generated by other thrusters, as represented in Figure 4. 20. The main simplification in this solution is that no interaction between currents is considered before its combination in the entrance of the thruster.

Figure 4. 20 – Combination of natural current and induced currents.

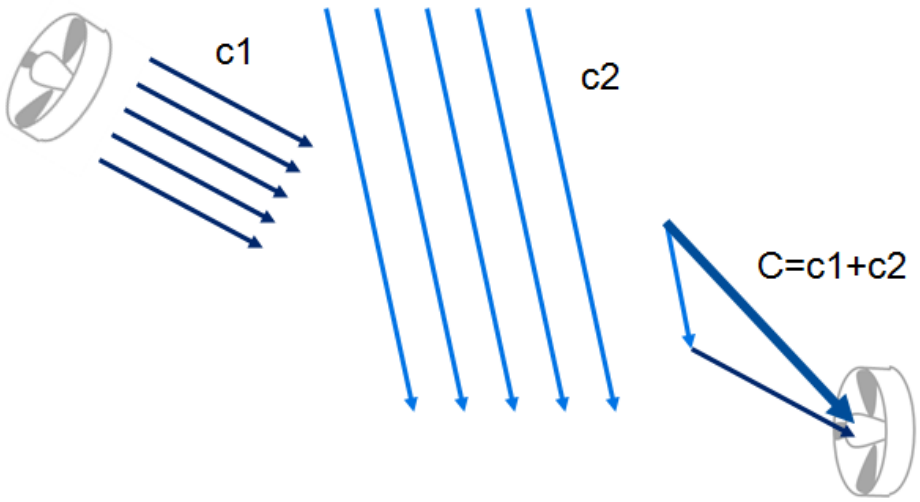

Source: Elaborated by the author.

4.2.2. Wake flow

In order to calculate the effects of the wake flow phenomena in the net thrust delivered by an azimuth thruster an efficiency curve is defined. The efficiency is defined as the ratio between the delivered thrust (T) considering the thruster in the

vessel (with all the implied interactions) and the thrust operating in open water (bollard pull - T_B), as represented in:

$$\eta = \frac{|T|}{T_B} \tag{4.11}$$

Note that the efficiency curve must be developed in polar coordinates in order to represent the azimuth thruster, since it can rotate 360º, and for every azimuth angle, the efficiency reduction should change, due to the different direction of the jet stream. Figure 4. 21 presents an example of an efficiency curve.

Figure 4. 21 – Azimuth thruster representation considering its efficiency and ideal representation.

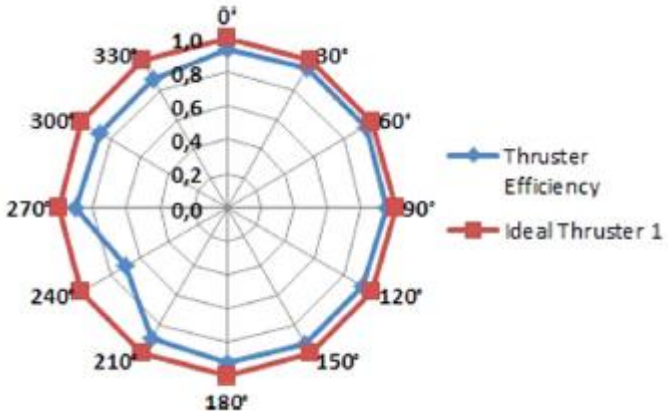

Source: Elaborated by the author.

The calculation of the efficiency curve can be performed according to the three methods discussed in section 4.1.1. Nevertheless, it is important to emphasize that model tests have already presented excellent results in order to determine the efficiency curve. Arditti *et al.* (2015) presents a thorough explanation of the method and the results of a thrust test conducted with a barge model.

4.3. Effects on the thrust allocation problem

Once the method for considering the hydrodynamic interactions quantitatively is defined, it is important to demonstrate how they affect the thrust allocation problem.

4.3.1. Power Calculation

As explained in the previous sections, the change in the inflow of the thruster affects its torque coefficient (c_Q), therefore its required power. Eq. 4.12 shows how the power equation is affected by the torque coefficient. Note that c_i is a constant value that depends on the water density and the diameter of the thruster, c_{Q_i} is the current torque coefficient and $c_{Q_{B_i}}$ is the torque coefficient in bollard pull conditions.

$$P_i = c_i(\rho, D) \cdot T_i^{\frac{3}{2}} \cdot \frac{c_{Q_i}}{c_{Q_{B_i}}} \tag{4.12}$$

The thrust allocation algorithms found in the bibliographic review always consider the term c_Q as a constant value. In order to enhance the thrust allocation regarding power consumption the torque coefficient should be considered. It can be done by calculating the relation $\frac{c_{Q_i}}{c_{Q_{B_i}}}$ at the beginning of each time step to better represent the power consumed by each thruster.

This approach can be also justified for the fact that advance ratio (J) will not change significantly between two time-step allocations, because the rate of change of azimuth angle ($\dot{\alpha}_{max}$) and the acceleration of the paddles of the thrusters ($\dot{n}_{max}$) are limited.

4.3.2. Thrust Calculation

In order to obtain the effective thrust delivered, the hydrodynamic interactions must be considered.

Observe that the inflow phenomena affect the thrust coefficient of the thruster. Eq. 4.13 shows how the delivered thrust (T_d) is affected by the thrust coefficient. Note that T_B is the thrust delivered in a bollard pull condition, c_{T_i} is the current thrust coefficient and $c_{T_{B_i}}$ is the torque coefficient in bollard pull conditions.

$$T_d = T_B \cdot \frac{c_{T_i}}{c_{T_{B_i}}} = T_B \cdot \eta_{inflow} \tag{4.13}$$

Furthermore, the Wake flow phenomena affect the delivered thrust. The effective thrust (T_{eff}) is calculated according to Eq. 4.14, where T_d is the delivered thrust and $\eta(\alpha)$ is the efficiency reduction due to Wake flow phenomena.

$$T_{eff} = T_d \cdot \eta(\alpha) = T_d \cdot \eta_{Wake\ flow} \tag{4.14}$$

Finally, the effective thrust can also be seen as the bollard pull thrust affected by inflow and wake flow phenomena, as represented in Eq. 4.15.

$$T_{eff} = T_B \cdot \eta_{inflow} \cdot \eta_{Wake\ flow} \tag{4.15}$$

4.4. Modelling physical limitations

The model adopted to represent the physical limitations is presented in Figure 2. 8. The following section presents the calculations necessary to quantitatively obtain these boundaries. Observe that the calculation of the physical limitations always depends on the previous state of the thrusters.

The maximum azimuth angle variation is represented in Eq. 4.16, where $\dot{\alpha}_{max}$ is the maximum rate of turn of the azimuth angle and Δt is the time interval of each time step of the time domain simulation.

$$\Delta\alpha_{max} = \dot{\alpha}_{max} \cdot \Delta t$$
$$\Delta\alpha_{max} - \alpha_0 \leq \alpha \leq \Delta\alpha_{max} + \alpha_0 \tag{4.16}$$

The maximum variation of thrust is shown in Eq. 4.17. Note that the first step is defining the present rotation of the Thruster. With the current speed of rotation it is possible to determine the lower (T_L) and higher (T_H) boundaries based on the maximum acceleration of the thruster ($\dot{n}_{max}$) and the time interval (Δt).

$$n_0 = \sqrt{\frac{T}{C_{T0} \cdot \rho \cdot D^4}}$$
$$T \geq T_L = C_{T0} \cdot \rho \cdot D^4 \cdot (n_0 - \dot{n}_{max} \cdot \Delta t)^2 \tag{4.17}$$
$$T \leq T_H = C_{T0} \cdot \rho \cdot D^4 \cdot (n_0 + \dot{n}_{max} \cdot \Delta t)^2$$

Furthermore, the saturation of the thrusters also sets a higher boundary. The calculation of the maximum thrust is presented in Eq. 4.18, where n_{max} is the maximum speed of rotation of the thruster.

$$T \leq T_{sat} = \ C_{T0} \cdot \rho \cdot D^4 \cdot {n_{max}}^2 \tag{4.18}$$

4.5. Thrust Allocation Problem

Once each part of the problem has been modeled separately it is important to finish this section presenting the thrust allocation modelled fully represented as an optimization problem (Eq. 4.19). Note that in this formulation it is clear that the optimization variables are

$$\Lambda = P = \min_{T,\alpha} \sum_{i=1}^{n} c_i(\rho, D) \cdot T_i^{\frac{3}{2}} \cdot \frac{C_{Q_i}}{C_{Q_{B_i}}}$$

$$R: \begin{cases} \sum_{i=1}^{N} T_i \cdot \cos(\alpha_i) \cdot \eta_{inflow_i} \cdot \eta_{Wake\ flow_i} - F_x = 0 \\ \sum_{i=1}^{N} T_i \cdot \sin(\alpha_i) \cdot \eta_{inflow_i} \cdot \eta_{Wake\ flow_i} - F_y = 0 \\ \sum_{i=1}^{N} \left[T_i \cdot \eta_{inflow_i} \cdot \eta_{Wake\ flow_i} \cdot (x_i \cdot \sin \alpha_i - y_i \cdot \cos \alpha_i) \right] - M_z = 0 \end{cases} \tag{4.19}$$

$$I: \begin{cases} \alpha \geq \alpha_0 - \Delta\alpha_{max} \\ \alpha \leq \Delta\alpha_{max} + \alpha_0 \\ T \geq T_L \\ T \leq T_H \\ T \leq T_{sat} \end{cases}$$

5. DEVELOPMENT OF THE THRUST ALLOCATION ALGORITHM

In this chapter the development of a thrust allocation algorithm is described. Initially the thrust allocation problem is modelled with slack variables. A review of the main optimization methods is presented to justify the selection of the SQP technique. Finally, the structure of the optimization algorithm is defined with all mathematical development.

5.1. Modelling the Problem with Slack Variables

In the previous chapter, the thrust allocation problem was modelled considering its mechanical characteristics, such as power generation, hydrodynamic interactions and physical limitations. Although not part of the mechanical characteristics the slack variables (*s*) are important for the solution when the thruster saturation prevents the vessel from generating the forces required by the control system. The incorporation of such variables leads to:

$$\Lambda = \min_{T,\alpha,s}\left\{\sum_{i=1}^{n} c_i(\rho, D)\cdot T_i^{\frac{3}{2}}\cdot\frac{C_{Q_i}}{C_{Q_{B_i}}} + s^T Q s\right\}$$

$$R:\begin{cases}\displaystyle\sum_{i=1}^{N} T_i\cdot\cos(\alpha_i)\cdot\eta_{inflow_i}\cdot\eta_{Wake\ flow_i} - F_x + s_1 = 0\\ \displaystyle\sum_{i=1}^{N} T_i\cdot\sin(\alpha_i)\cdot\eta_{inflow_i}\cdot\eta_{Wake\ flow_i} - F_y + s_2 = 0\\ \displaystyle\sum_{i=1}^{N}\left[T_i\cdot\eta_{inflow_i}\cdot\eta_{Wake\ flow_i}\cdot(x_i\cdot\sin\alpha_i - y_i\cdot\cos\alpha_i)\right] - M_z + s_3 = 0\end{cases} \tag{5.1}$$

$$I:\begin{cases}\alpha \geq \alpha_0 - \Delta\alpha_{max}\\ \alpha \leq \Delta\alpha_{max} + \alpha_0\\ T \geq T_L\\ T \leq T_H\\ T \leq T_{sat}\end{cases}$$

As previously mentioned the slack variables relax the problem, which means that the equalities (R) can always be achieved, considering the inequalities (I). This approach makes the problem robust, since without the slack variables, in case the forces required by the control system were too high or rapidly changed, it would not be possible to match them, and the thrust allocation algorithm could not provide results.

Using slack variables provides another advantage. The weight matrix Q can be used to define priorities for the errors in different directions. Observe that in a normal situation, the objective function will be minimized and the slack variables will be null (meaning no error). In adverse scenarios, where it is not possible to match the control forces, it will not be possible to have all the slack variables null. By defining different weights for each of the slack variables (by means of the matrix Q). It is possible to prioritize the error minimization in the yaw direction. This enables us to keep the vessel from turning, which could lead to higher environmental forces, since it is usually aligned in the weathervane direction (position that minimizes the environmental loads).

Eq. 5.2 presents the calculation for the weight factors; observe that they relate the power of the vessel at the current state (P), which is also in the objective function, and the required forces and moment in each of the directions (F_x, F_y, M_Z), squared. This is done in order to equalize the units of the objective function (P and $s^T Q s$); moreover, it allows directly relating the importance of the error and power minimizations. Note that the weights Q will therefore define the priorities of this multiobjective function, which implicitly contains the following objectives: accurate force generation and power minimization. The scalar weight values will generally have high values in order to increase the importance of the main objective of the thrust allocation, which is correct force generation, followed by power minimization.

$$Q = \begin{bmatrix} Q_1 \dfrac{P_0}{{F_x}^2} & 0 & 0 \\ 0 & Q_2 \dfrac{P_0}{{F_y}^2} & 0 \\ 0 & 0 & Q_3 \dfrac{P_0}{{M_z}^2} \end{bmatrix} \tag{5.2}$$

Note that if F_x, F_y or M_z are equal to 0. A minimum value should be used to avoid a singularity. This minimum value should not be too small that an error in a direction where the vessel is not requested takes priority over all the other directions.

5.2. Optimization Methods

There are several optimization methods, which are presented and categorized in Figure 5. 1, followed by a brief discussion of their main characteristics. For more information see Silva (2011) and Nocedal and Wright (2006).

Figure 5. 1 – Optimization Methods.

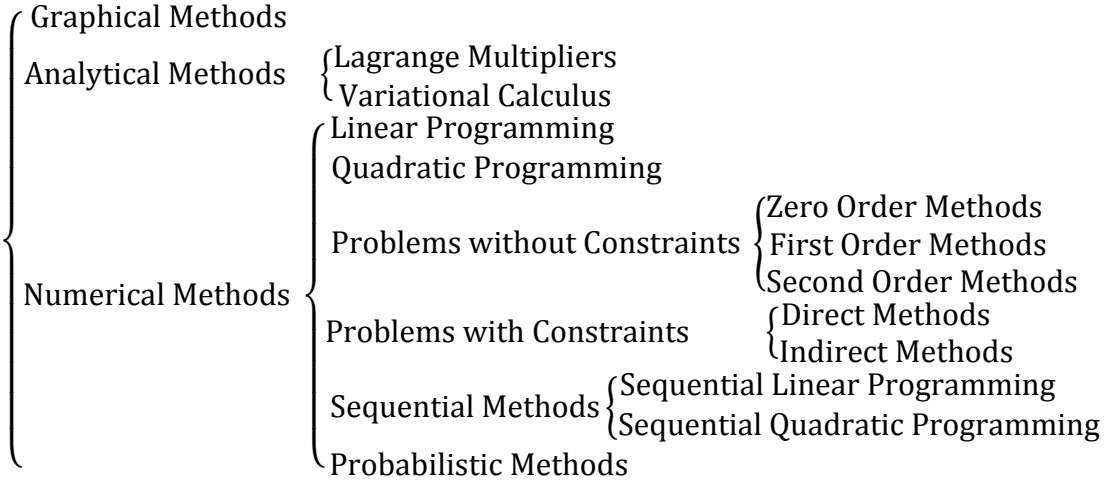

Source: Elaborated by the author.

The graphical method consists of representing the viable space (the constraints) and contours of the objective function, followed by a search for the optimal points. Although it is an efficient method it is very simple and does not allow solving problems with more than two degrees of freedom.

Analytical methods are the most consistent, that is, their results are reliable because they are based on purely mathematical solutions. However, if the optimization problem is moderately complex, it is not possible to use such methods.

In this class, the Lagrange multipliers method and the Variational Calculus, commonly used in structural problems, stand out.

Numerical methods present a wide range of optimization techniques. The linear programming method, for example, is widespread, but it is only applicable for linear optimization problems (with linear objective function and linear constraints).

Unrestricted problems provide great freedom for searching the solution. The difference between the zero order, first order and second order methods is the level of information from the objective function. Zero-order methods work with values of the objective function. First order methods work also with the information from the gradient of the objective function. And second order methods have also information of the hessian of the objective function.

Nonlinear constrained optimization problems are quite complex. There are mainly two approaches to solving them: “walking” within the viable space with information about the objective function gradient and verifying whether each step has improved the solution (direct methods) or; Transform a problem with constraints into an unrestricted problem (indirect methods), e.g. by applying a penalty function (incorporated in the objective function) when a constraint is not respected and remove the constraint from the problem, allowing the application of an unrestricted method to solve the modified problem.

The sequential methods approximate the nonlinearities of the problem by “well behaved” functions (generally linear and quadratic). The simplified problem is then solved by well-established linear and quadratic programming methods. Note that the simplifications are only applicable to the interval where the approximations are valid, generally an interval of the complete viable space. Therefore, the problem should be sequentially approximated and solved, until a convergence is obtained.

The probabilistic methods try to solve the optimization problems through random solutions. Examples of this line are solvers inspired on natural behavior, such as genetics and animal comportment, since these behaviors were naturally selected (optimized). Probabilistic methods are easy to solve, since they require only evaluations of the objective function. However, they are costly because they require a significant amount of optimal candidates until the solution is obtained.

5.2.1. Selection of Optimization Method

Considering the constrained nonlinear characteristics of the thrust allocation problem (Eq. 5.1), simpler algorithms are clearly not applicable to solve it. From the selection of optimization methods presented in Figure 5. 1, the viable candidates are: direct and indirect methods, sequential programming techniques and probabilistic algorithms.

From this selection, the sequential methods are clearly the fittest to solve the thrust allocation problem. Within their strong characteristics are the efficiency in which nonlinear and non-convex problems are solved, which is significantly relevant to this problem. Moreover Table 5. 1 presents the reasons why the other methods are not adequate to solve the thrust allocation problem.

Table 5. 1 – Reasons to not use some optimization methods to solve the thrust allocation problem.

Optimization Method	Reason it is not applicable to solve thrust allocation.
Direct Methods	The nonlinear charactristics of the problem prevent its analytical solution.
Indirect Methods	The amount of constraints and their nonlinear characteristics (specially equality constraints) prevent the application of these methods, because transporting all of them to the objective function would create a highly nonlinear multiobjective function, in which the weight definition for each objective would drastically change the optimal solution, and the definition of the optimal solution would not be clear.
Probabilistic Techniques	The Dynamic Positioning system requires that the thrust allocation problem is solved efficiently with regards to the time execution of the algorithm. Therefore, probabilistic techniques, which require numerous evaluation of probable optimal candidates are not adequate for real time applications.

From the selection of sequential methods, the SQP technique is chosen due to its higher similarity with the objective function, when compared to the linear approach.

5.3. Thrust Allocation Algorithm

The developed thrust allocation algorithm is presented in Figure 5. 2. Observe that it follows the structure of the SQP technique. In this section the algorithm is further detailed.

Figure 5. 2 – Structure of the developed thrust allocation algorithm.

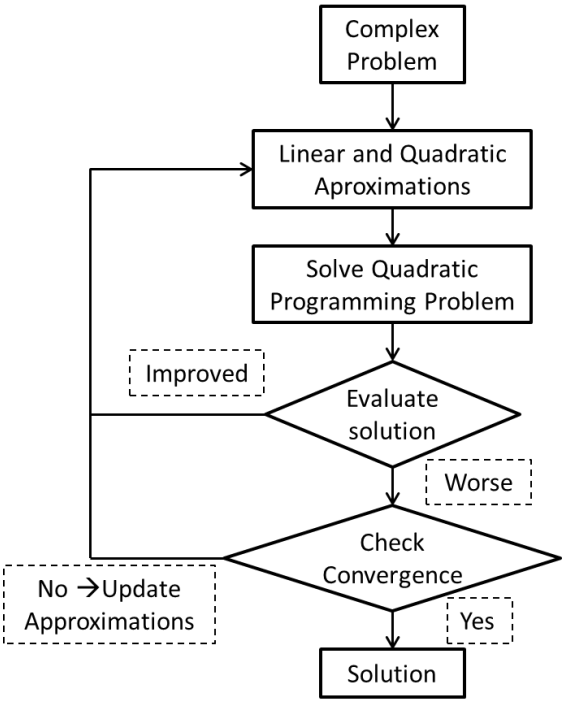

Source: Arditti, et al (2018a).

The SQP method is detailed presented in Nocedal and Wright (2002) and the application of this method to solve thrust allocation problems is presented in Arditti et al. (2015). Briefly, the SQP method consists of the following steps:

1) Approximating the objective function by a quadratic equation (Λ_Q) and approximating the nonlinear equalities by a set of linear equations (R_L).

Observe that locally approximating the problem is performed in the current state (previous solution) using the Taylor approximation method.

$$\Lambda_Q = \sum_{i=1}^{N} c_i \cdot {T_0}_i^{\frac{3}{2}} + \sum_{i=1}^{N} \frac{\partial \left(c_i \cdot T_i^{\frac{3}{2}} \right)}{\partial T_i} \cdot \left(T_i - {T_0}_i \right) + \frac{1}{2} \cdot \sum_{i=1}^{N} \frac{\partial^2 \left(c_i \cdot T_i^{\frac{3}{2}} \right)}{\partial {T_i}^2} \cdot \left(T_i - {T_0}_i \right)^2 + s^T Q s \quad (5.3)$$

$$R_L = R(T_0, \alpha_0) + \sum_{i=1}^{N} \frac{\mathrm{d}R(T_0, \alpha_0)}{\mathrm{d}T_i} \left(T_i - {T_0}_i \right) + \sum_{i=1}^{N} \frac{\mathrm{d}R(T_0, \alpha_0)}{\mathrm{d}\alpha_i} \left(\alpha_i - {\alpha_0}_i \right) + s \quad (5.4)$$

2) Solving the local Quadratic Programming (QP) problem. Note that many solutions have already been developed to this class of problems. Therefore, approximating the thrust allocation problem by a quadratic optimization is very interesting. In this study, the QP problem is solved with the Active-set algorithm. The work of Arditti et al. (2015) presents a graphical illustration of this method.

3) From the new solution, repeating the steps above, using a convergence factor to stop the process.

Note that the limit for the approximations (step 1) is the interval defined by the physical limitations (I). This procedure guarantees that the solution stays within this important constraint.

5.4. Discussion of relevant optimization aspects

5.4.1. Convexity

THRUST ALLOCATION PROBLEM

Convexity is an optimization property that guarantees that a local minimum is the global minima (Nocedal and Wright 2002). For an optimization problem to be convex, it should have convex objective function and constraints.

In order for the objective function to be convex, its Hessian Matrix (Eq. 5.5) must be positive semi-definite or definite. In practical terms this means that the eigenvalues of the Hessian Matrix must all be greater than or equal to 0. Note that

the Hessian matrix of the objective function of the thrust allocation problem is convex, since the eigenvalues are 0 or $\frac{3}{4\sqrt[2]{T}}$. This is an easy calculation because the diagonal of the Hessian Matrix is filled with $\frac{3}{4\sqrt[2]{T_1}}$, 0, $\frac{3}{4\sqrt[2]{T_2}}$, 0... and all the other values are null.

$$Hess = \begin{bmatrix} \frac{\partial^2 \lambda}{\partial {x_1}^2} & \frac{\partial^2 \lambda}{\partial x_1 \partial x_2} & \cdots \\ \frac{\partial^2 \lambda}{\partial x_2 dx_1} & \frac{\partial^2 \lambda}{\partial {x_2}^2} & \cdots \\ \vdots & \vdots & \ddots \end{bmatrix}$$

$$Hess = \begin{bmatrix} \frac{3}{4\sqrt[2]{T_1}} & 0 & 0 & 0 & \cdots \\ 0 & 0 & 0 & 0 & \cdots \\ 0 & 0 & \frac{3}{4\sqrt[2]{T_2}} & 0 & \cdots \\ 0 & 0 & 0 & 0 & \cdots \\ \vdots & \vdots & \vdots & \vdots & \ddots \end{bmatrix} \quad (5.5)$$

For the domain to be convex, the inequality constraints must be concave. And the equality constraints must be linear. Physically this means that in a convex domain, if we join two points inside it, by a line segment ($\vec{r}$), all points of ($\vec{r}$) are inside the feasible domain.

Figure 5. 3 presents the physical interpretation of convex and non-convex domains. Observe that the thrust region of a thruster, considering the wake flow interactions is clearly a non-convex domain.

Figure 5. 3 – Convex and non-convex viable spaces.

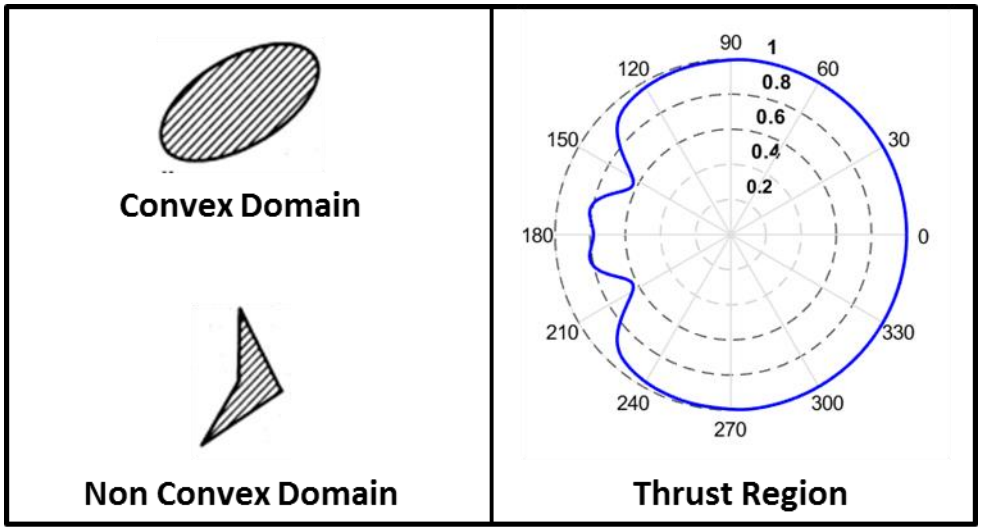

Source: Elaborated by the author.

Therefore, the thrust allocation problem considering hydrodynamic interactions is a non-convex problem. This result is expected, considering that the hydrodynamic interactions can significantly influence the thrust generation, and the shape of the hull and underwater equipment varies from vessel to vessel.

However, when considering the physical limitations of the thrusters, observe that the actual thrust region is only a small part of the domain presented in Figure 5. 3. This domain is in general convex, except in areas where the wake flow interaction has a significant influence on the thrust generation.

Although there is no guarantee that the solution found by the SQP algorithm is the global minima (since the problem is non-convex), the solution found is optimal, or close to optimal, in most cases, when considering the following characteristics of the simulations presented in previous works:

- In Arditti and Tannuri (2011), it can be observed that the developed thrust allocation algorithm using efficiency functions to represent wake flow interactions, avoid zones where significant interaction occurs. These zones are generally non-convex, as illustrated in Figure 5. 3.
- In Arditti et al. (2014) a simulation when the thrusters need to cross the area of significant wake flow interaction, normally considered a

forbidden, shows that this procedure is performed with the following optimal procedure:

- The thruster stops in the border of the zone with high wake flow interaction.
- Lower significantly the generated thrust.
- Cross the zone low efficiency zone as fast as possible.
- Increase the generated thrust and reposition itself in the optimal direction following the required forces.

APPROXIMATED PROBLEM

An additional discussion over convexity is relevant for the approximated problem. Observe that the objective function is approximated by Eq. 5.3, which is convex, since its eigenvalues are all higher or equal to 0.

The nonlinear equality constraints are linearly approximated by Eq. 5.4. Linear functions are by definition convex. The same is valid for the inequalities, which are all linear.

The convexity characteristic of the approximated problem, guarantees that the local minima found by the active-set algorithm, is the global minima.

SLACK VARIABLES

The slack variables were not included in the convexity analysis in order to make it simpler. Note that the slack variables are convex, both in the objective function (because matrix Q is positive definite) and on the constraints (linear functions).

5.4.2. Varying Limits

The use of varying limits is not usual in the SQP method. However, it is an interesting solution because the Hessian of the objective function (Eq. 5.5) presents

null eigenvalues. The null eigenvalues refer to the contribution of the azimuth angles in the power consumption, which are of course null. Therefore, if the varying limits were not used, the QP algorithm would vary the azimuth angles infinitely to match the linearized equalities, which would not solve the allocation problem. Furthermore, the varying limits can be used to define the range for the simplifications performed by the SQP method.

The implementation of the varying limits in the SQP method is carried out according to the following procedure: An interval of simplification is initially defined; if it is too large, it leads to bad approximations and solutions. If that is the case, the range of approximations is diminished (varying limits) and a better solution can be found. This procedure is repeated until the varying limits are significantly small.

The varying limits are also limited by the physical limitations of the thrusters (inequalities I). This procedure guarantees that the solution stays within this important constraint.

6. CASE STUDY

In this chapter a case study is presented. Initially data from the vessel model, efficiency functions and relevant information of interaction effects is described. Once the model is defined, the method used to perform time domain simulations is discussed.

Defined all the parameters for the case study, interesting simulation cases are presented and discussed. The discussions of the results are presented together with a small conclusion for each case, in order to guarantee better understanding of the optimization algorithm behavior in different situations.

6.1. Vessel Model

BGL1 is a crane and pipe-laying barge (Figure 6. 1), operating in Brazilian waters for more than 20 years. Equipped with a conventional mooring system and operated with the aid of anchor handling tugboats, BGL1 was originally designed for shallow and intermediate depths. It was modified for offshore operations, such as pipe laying and equipped with a DP system (Tannuri *et al.* 2002). Main data of the barge is presented in Table 6. 1.

Figure 6. 1 – BGL1 with a supply boat at portside.

Source: Tannuri *et al.* (2002).

Table 6. 1 – BGL main data.

Length (L)	$121.9\ m$
Beam (B)	$30.48\ m$
Draft (T)	$5.18\ m$
Mass (M)	$17177\ ton$
Surge Added Mass (M_{11})	$1717\ ton$
Sway Added Mass (M_{22})	$8588\ ton$
Yaw Added Mass (M_{66})	$1.27 \cdot 10^7\ ton\ m^2$
Lateral Area (AL)	$1500\ m^2$
Frontal Area (AF)	$420\ m^2$

The thrusters considered in the simulation have the same characteristics as presented on the 4-quadrant diagram (Figure 2. 5). The location and maximum thrust of each thruster are presented in Table 6. 2. Observe that these are not the actual thrusters of the vessel, however they are used for the simulation due to the amount of data available; note that the original thrusters also have a curve for thrust and torque coeficient with relation to the advance speed ratio.

Table 6. 2 – Thruster positions and maximum bollard pull thrust.

Thruster	x axis	y axis	Max. Thrust
1	-50.6 m	0.0 m	330 kN
2	-40.7 m	-9.8 m	330 kN
3	-40.7 m	9.8 m	330 kN
4	36.3 m	9.8 m	330 kN
5	36.3 m	-9.8 m	330 kN
6	46.1 m	0.0 m	330 kN

Figure 6. 2 presents the efficiency curves of the vessel, where the wake flow efficiency of all thrusters of the vessel is illustrated. For example, considering thruster 1, observe that there is significant loss of efficiency when it operates in positions

where its wake flow interacts with other thrusters (2 and 3) or with the hull of the vessel.

Figure 6. 2 – Polar plot of Wake flow efficiency for all the thrusters.

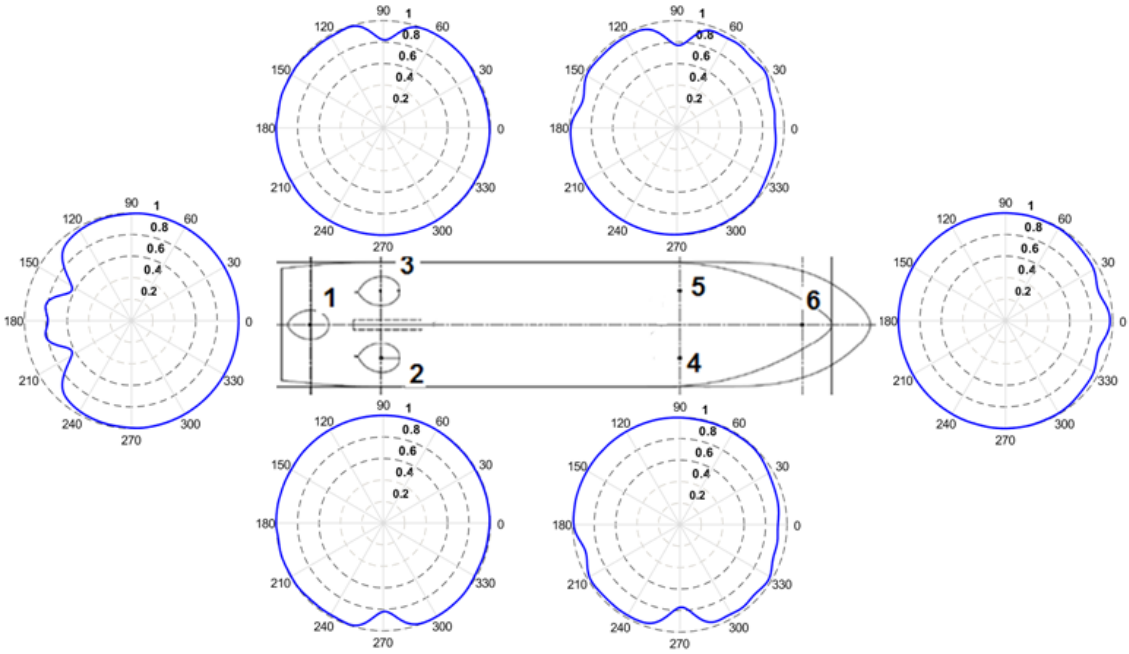

Source: Arditti, et al (2018).

6.2. Simulation Model

The simulations are executed using the Dynasim, a time domain numerical simulator developed by Petrobras in co-operation with Brazilian universities. It was designed for the analysis of moored and DP offshore systems. The mathematical model of the Dynasim and validation results are presented in Nishimoto et al. (2002), Tannuri and Morishita (2006), Tannuri et al. (2009). A customized version of the simulator was used throughout the simulations presented in this thesis, which allows the integration with specific control and allocation algorithms.

The barge dynamics are simulated in the horizontal plane, considering surge, sway and yaw axis. The following dynamic model gives horizontal motions of the barge (Tannuri *et al.* 2002):

$$\begin{aligned}(M + M_{11})\dot{x}_1 - (M + M_{22})\dot{x}_2\dot{x}_6 - M_{26}\dot{x}_6{}^2 &= F_{1E} + F_{1O} + F_{1T}\\ (M + M_{22})\ddot{x}_2 + M_{26}\ddot{x}_6 + (M + M_{11})\dot{x}_1\dot{x}_6 &= F_{2E} + F_{2O} + F_{2T}\\ (I_Z + M_{66})\ddot{x}_6 + M_{26}\ddot{x}_2 + M_{26}\dot{x}_1\dot{x}_6 &= F_{6E} + F_{6O} + F_{6T}\end{aligned} \quad (6.1)$$

Where $M_{i,j}$ is the additional mass in the direction i,j; I_Z is the moment of inertia about the vertical axis; F_{1E}, F_{2E}, F_{6E} are surge, sway and yaw environmental loads (current, wind and waves), see Tannuri *et al.* (2002) for further details on how they are calculated. F_{1O}, F_{2O}, F_{6O} are operation forces and moment used to simulate an offshore operation, they are equal to the forces applied on the vessel by a pipe lay operation. F_{1T}, F_{2T}, F_{6T} are the net forces and moment delivered by the propulsion system. The variables $\dot{x}_1$, $\dot{x}_2$ and $\dot{x}_6$ are the midship surge, sway and yaw absolute velocities.

The DP system is equal to the one represented in Figure 2. 3. A feedback linearization controller (Slotine and Li, 1991) was implemented in the simulator, based on the “inverse” of the non-linear dynamics of the barge. The feedback linearization technique allows “cancelling” the nonlinear part of the dynamics, making it possible to design a simple controller based on a proportional derivative (PD) law to move the ship towards its requested position (Tannuri *et al.* 2002).

A feedforward controller was designed to counteract wind forces and a wave filter was included to attenuate the 1st order variation on the measured signals.

The simulations are performed in Simulink ®. The quadratic programming problem is solved with the routine QuadProg from Matlab ®.

The simulations performed considered all the actuator physical limitations, namely: $T_{sat} = 330\ kN$, $\dot{\alpha}_{max} = 12^{\circ}/s$, $\dot{n}_{max} = 1 rad/s^2$. Observe that these values are in accordance with data found in the available bibliography (Tannuri et al. (2012) and Thrustmaster Inc. Technical Specification), representing a sufficient model to describe the actuator dynamic effects (DNV 2016 and Karlsen, Pivano and Ruth 2016).

Furthermore, it is worth mentioning that the variables used to determine interaction between thrusters are: spread angle ($\theta = 5°$), the constant for energy flow

loss ($k = 10$), and the values of C_T and C_Q are in accordance with the 4 quadrant diagram presented in Figure 2. 5.

Finally, for the saturation simulation the following weight values were considered: $Q_1 = Q_2 = 100$ and $Q_3 = 5000$. And for the other simulations the following weight values were used: $Q_1 = Q_2 = 1000$ and $Q_3 = 10000$.

6.3. Saturation Simulation

In this simulation a time series of environmental forces acting on the vessel is increased in order to create a situation where it is not possible to generate the forces required by the control system, due to thruster saturation.

The result of the simulation is presented in Figure 6. 3. Observe that the thrust allocation algorithm was not able to generate the required forces in the sway direction during some periods. On the other hand, the surge force and the yaw moment (with higher precision) were correctly generated. The periods with higher error on sway force occur when the yaw moment reaches its maximum value, demonstrating that in this case, a choice between accurately generating the lateral force or the moment had to be done. As previously discussed, this choice is made when the weight matrix (Eq. 5.2) is defined. Since higher priority for the yaw moment was defined on the weight matrix, the thrust allocation algorithm keeps track of the required moment, despite some imprecision in the sway force.

Figure 6. 3 – Saturation simulation – Required and Delivered forces.

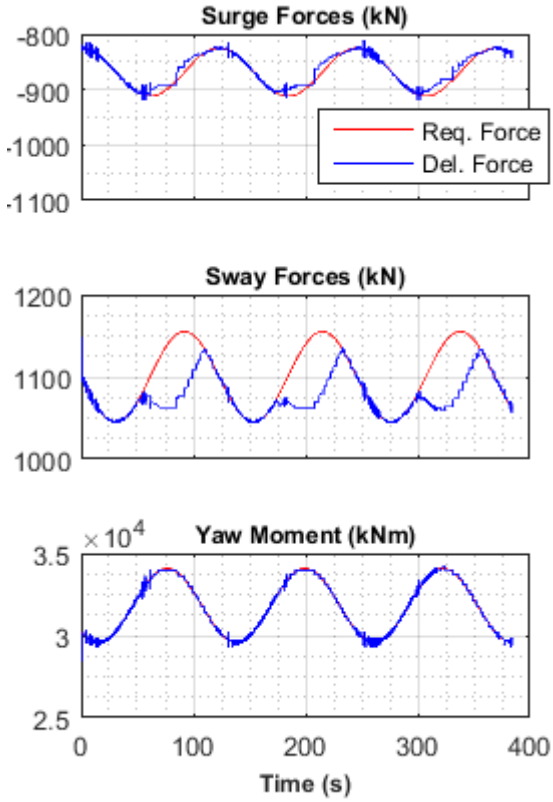

Source: Arditti, et al (2018).

Figure 6. 4 presents the allocations (thrust and azimuth angle) of the thrusters during the saturation simulation. The allocations are bounded by the physical limitations of the thrusters. All the thrusters of the vessel reached their maximum thrust (saturation) in some periods, which reveals that the thrust allocation algorithm is using all the available resources to match the required forces. Furthermore, these periods of total saturation correspond to the errors in force generation, meaning that the thrust allocation algorithm tries to match the required forces; when it is not possible, it tries to minimize the error, according to the predefined priority. This is exactly the robust behavior expected from the control system of DP vessels in extreme situations.

Figure 6. 4 – Saturation simulation – Allocations.

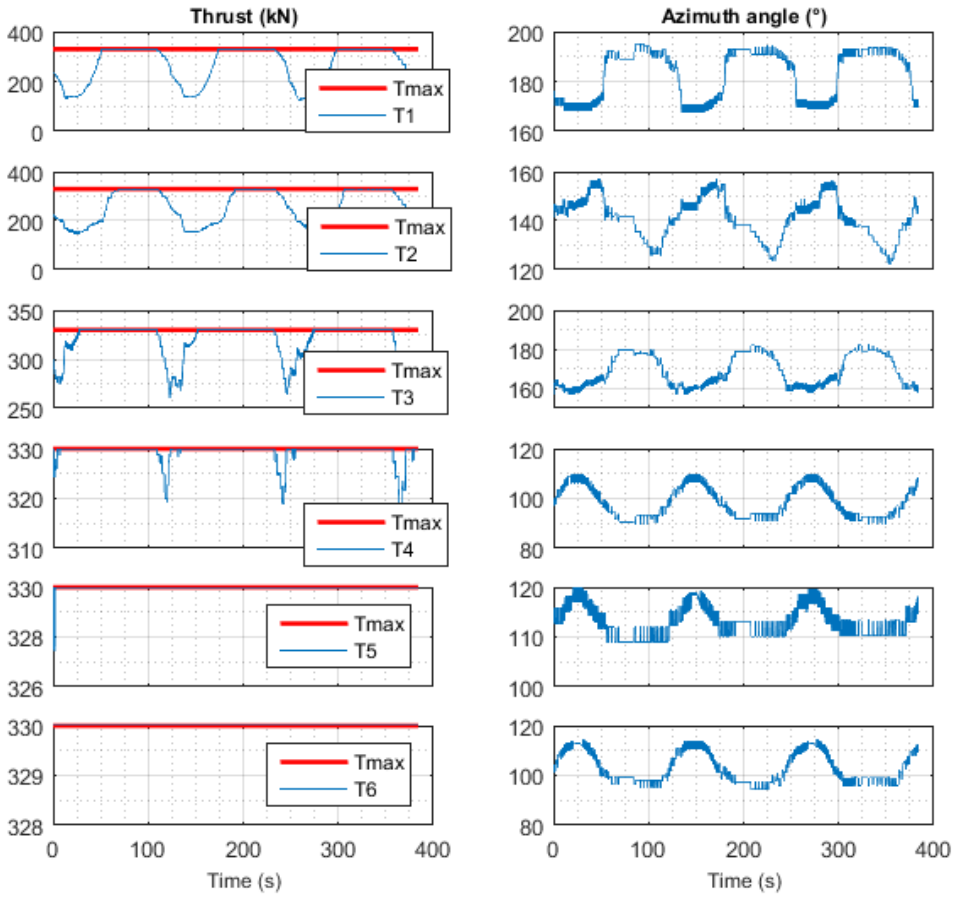

Source: Arditti, et al (2018).

The hydrodynamic interactions were considered according to the model described in modelling section, with the inflow and wake flow updated at every step of the optimization algorithm.

To illustrate how the hydrodynamic interactions, affect the thrust allocation algorithm, Figure 6. 5 presents the wake flow, inflow and combined efficiencies. Note that a natural current of $2\ m/s$ arriving from the bow was considered. The current is purposely exaggerated in order to demonstrate the algorithm behaviour and match the simulation objective (thruster saturation).

It is easy to identify the effect of the wake flow efficiency by comparing the azimuth angles of the thrusters during the allocation (Figure 6. 4) with the polar plot of wake flow efficiency of the thrusters (Figure 6. 2). Regarding the inflow efficiency, it is obtained by calculating the inflow current of each thruster (combination of natural

current and current induced by other thrusters) in combination with the speed of the thruster blades to obtain the advance speed (J). The advance speed is used to calculate β; which allows finding the thrust coefficient (C_T) on the 4-quadrant diagram; the thrust coefficient is divided by the bollard pull coefficient (C_{T_B}) as in Eq. 4.16, leading to the inflow efficiency. Finally, the combined interaction is the combination of the inflow and wake flow efficiencies ($\eta = \eta_{inflow} \cdot \eta_{Wake\ flow}$), as in Eq. 4.18.

Figure 6. 5 - Wake flow, inflow and combined interaction efficiencies.

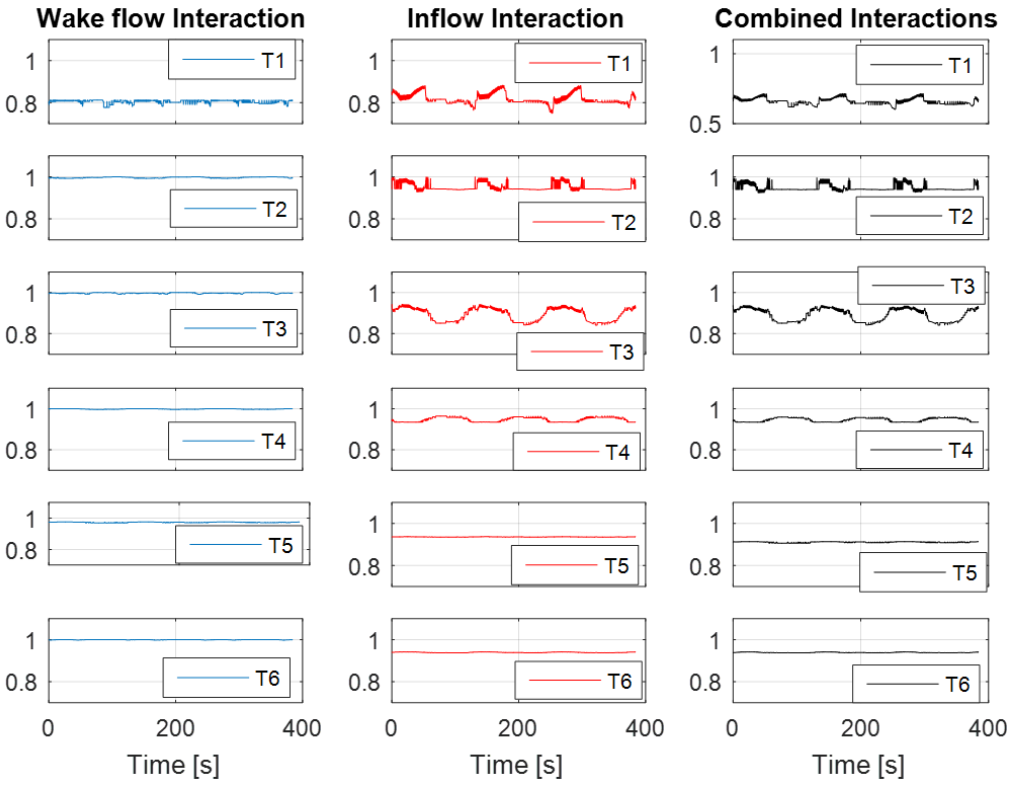

Source: Arditti, et al (2018).

Furthermore, the simulation considered a time step of 0.25 s. For every time step, the thrust allocation algorithm required at maximum 0.13 s to find the optimal solution (on an average computer with 8GB of ram memory and intel i7 – third generation processor). The processing time is observed to be very efficient, taking into account the complexity of the problem; it is therefore feasible to use this algorithm in real time simulations and operations.

The robust thrust allocation algorithm, programmed with a Sequential Quadratic Programming technique and slack variables, is able to efficiently solve the complex optimization (thrust allocation) problem. Furthermore, the strategy adopted allows a consistent response for situations in which it is not possible to generate the forces required by the control system, due to physical limitations of the actuators.

6.4. Offshore Operation Simulation

This simulation presents the control of the same vessel during an operation assisted by DP control. In this hypothetical offshore operation, a 900kN external pulling force acts on the vessel stern (similar to a pipe lay operation). The simulated sea-state is $1.2\ m/s$ current, $12\ m/s$ wind (10 min average) speed and waves with $2.0\ m$ significant height and $6.0\ s$ zero up-crossing wave period. A 90° incidence for wind and wave, with the vessel aligned with the current was considered, which represents the critical case for this vessel. Figure 6. 6 illustrates the simulated scenario.

Figure 6. 6 – Simulated offshore operation scenario.

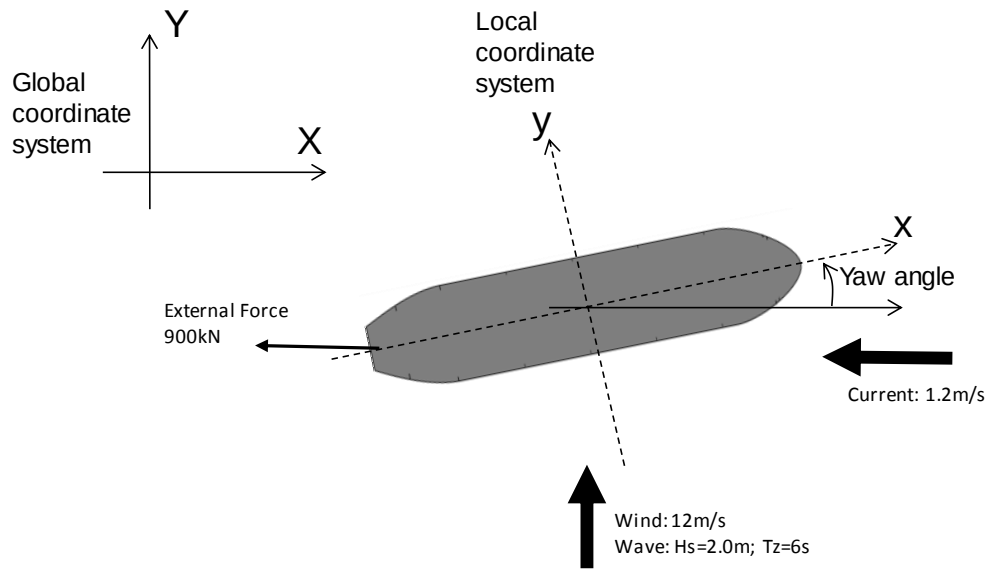

Source: Arditti, et al (2018).

The control set point was defined at the origin (X, Y, φ_{yaw}) = (0, 0, 0°). The hydrodynamic interactions were also considered according to the previously defined model.

In order to analyse the importance of considering the hydrodynamic interactions in the thrust allocation and the effects of this decision on the control system, two allocation algorithms were simulated. The first one is the SQP described in the previous section. The second one is a similar allocation technique where the hydrodynamic interactions are not considered. Note that once the allocation is determined, the real delivered forces are calculated considering all the hydrodynamic interactions, and this force vector is considered as the output of the vessel during the simulations.

Figure 6. 7 presents the simulation results for both algorithms. On the left side, the movements of the gravity centre and the heading of the vessel are compared; note that the algorithm considering the hydrodynamic interactions is able to keep the vessel closer to the origin (set point). This result is clearly observed on the right-side image, where the vessel gravity centre movements were represented in 2D. The average position of the vessel considering the hydrodynamic interactions (average distance to the origin: 0.1 m; maximum distance: 3.6 m) is significantly closer to the set point than the case in which the interactions are not considered (average distance to the origin: 4.4 m; maximum distance: 6.7 m).

Figure 6. 7 – Vessel movements during real operation simulation considering (and not) hydrodynamic interactions during the thrust allocation.

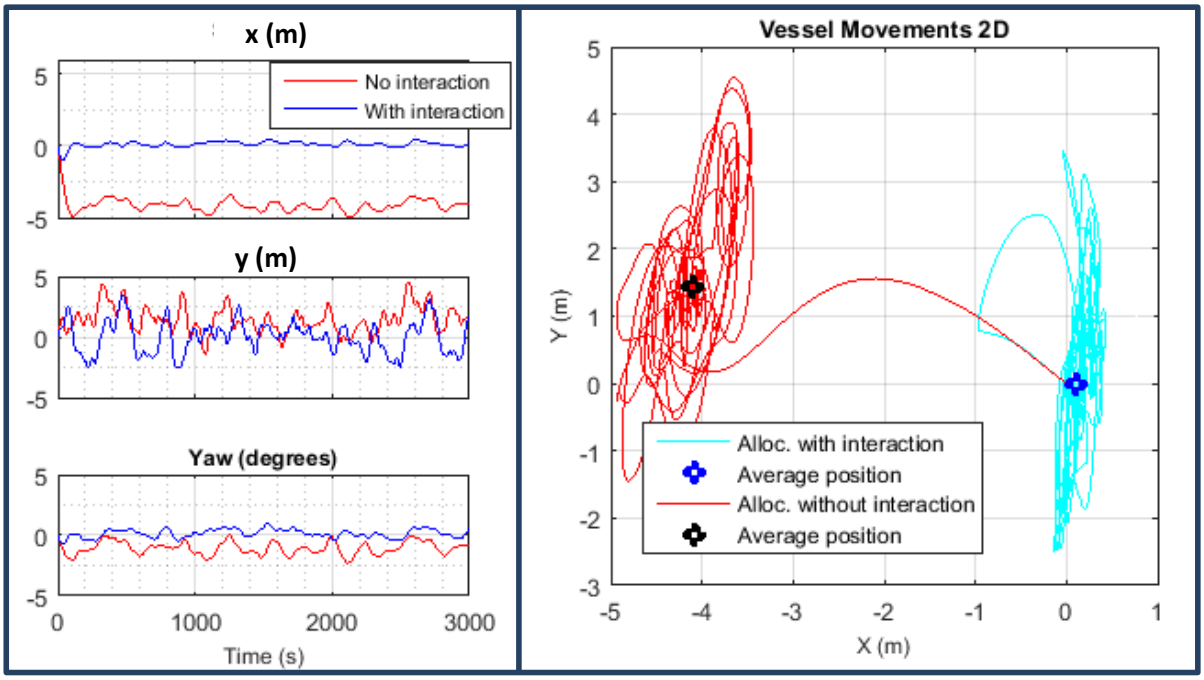

Source: Arditti, et al (2018).

Figure 6. 8 presents the positions of the vessel during the operation simulation. Note that other than coming further of the set point in Surge and Sway axis (Figure 6. 7), the algorithm that does not consider the hydrodynamic interaction has higher yaw movements and chattering.

Figure 6. 8 – Track of the vessel during operation simulation.

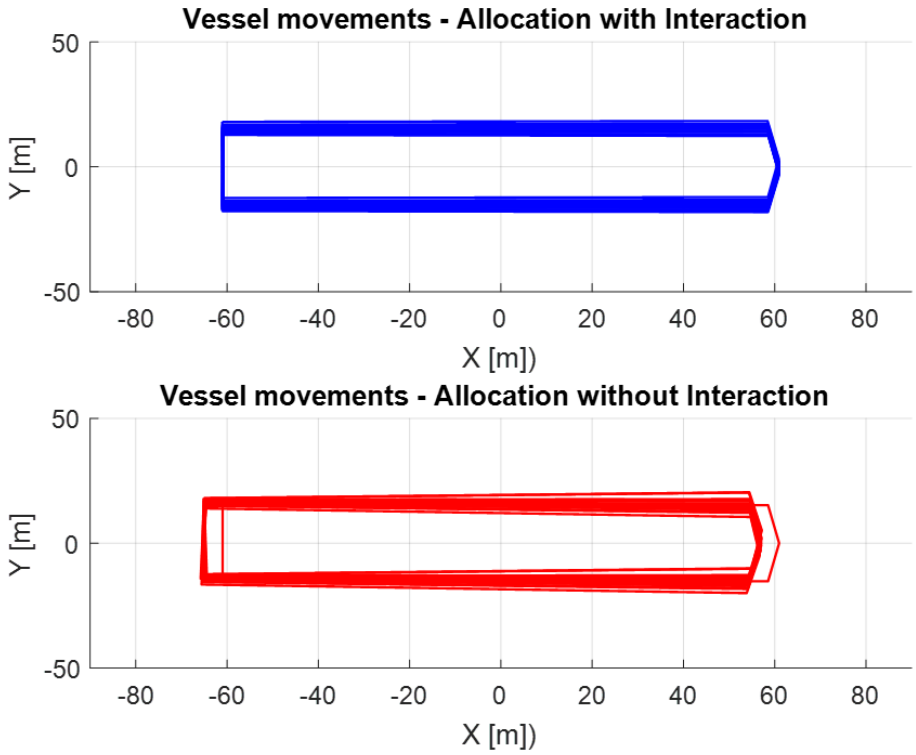

Source: Elaborated by the author.

Observe that the control system implemented does not contain an integral parcel of the error. Therefore, the imprecisions in force generation, of the thrust allocation algorithm that does not consider the hydrodynamic interactions, prevent the controller from bringing the vessel to the defined set point. In this case the higher force requirement occurred in surge direction, due to the 900kN external force; consequently, the larger regime error occurred in this direction, mainly because most of the thrusters of the vessel are pointed in this direction, but the thrust delivered is lower than the required due to the interactions. Figure 6. 9 illustrates the forces present in the simulation, namely: Wind, Wave, Current, External Force and Control.

Figure 6. 9 – Operation forces.

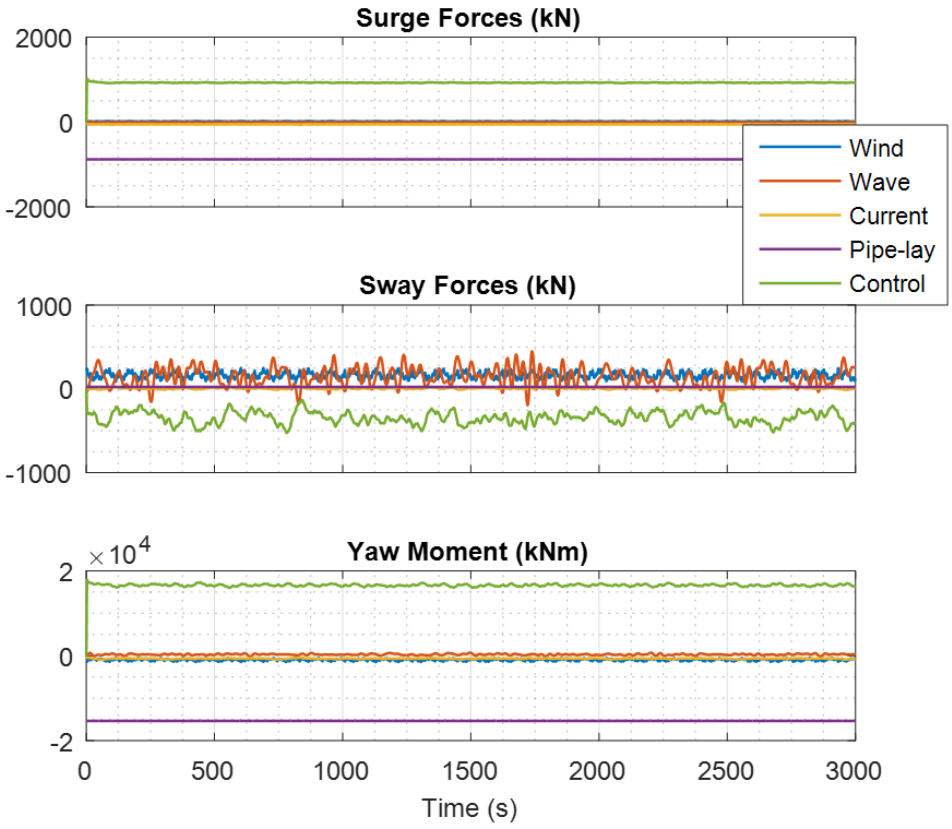

Source: Arditti, et al (2018).

The results of this simulation can easily be understood when the errors in force generation are compared (Figure 6. 10). Note that the algorithm that did not consider the hydrodynamic interactions had in average the following errors for surge, sway and yaw: 7%, 6% and 2%. Conversely the thrust allocation considering the interactions had approximately 0% error. Furthermore, the average power consumption of the algorithm considering the hydrodynamic interactions was equal to the algorithm that did not consider hydrodynamic interaction (0.05% less power required in average). Therefore, considering the hydrodynamic interactions on the thrust allocation improves the control system in terms of precision without additional power consumption.

Figure 6. 10 – Comparison of force generation errors for offshore operation simulation.

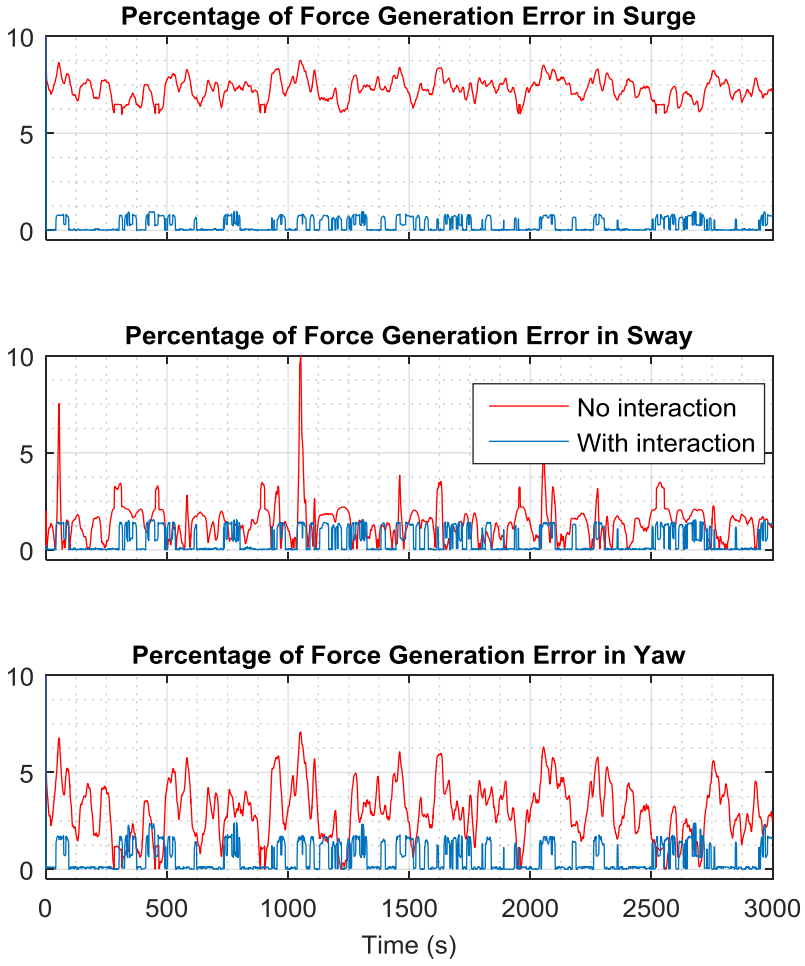

Source: Arditti, et al (2018).

Simulations with the vessel model, environmental conditions, complete DP system and a consistent hydrodynamic interaction model had never been carried out before. This methodology will bring improvements to the shipbuilding industry by more reliably simulating: general offshore operations (e.g. drilling assisted by DP), ship maneuvering and general navigation.

Furthermore, considering the hydrodynamic interactions in thrust generation will lead to more reliable and precise offshore operations.

6.5. Capability Plot of DP Simulations

This simulation presents the DP control of the vessel in a series of environmental conditions, each one with a different angle of attack of the environmental forces (wind, wave and current), without any external force simulating an offshore operation. This technique known as capability plot presents the behavior of the vessel for sea states approaching all around the vessel with discretion of 30°. The simulated sea-state is 1.2 m/s current, 12 m/s wind speed and waves with 2.0 m significant height and 6.0 s zero up-crossing wave period.

Figure 6. 11 – Simulated scenario.

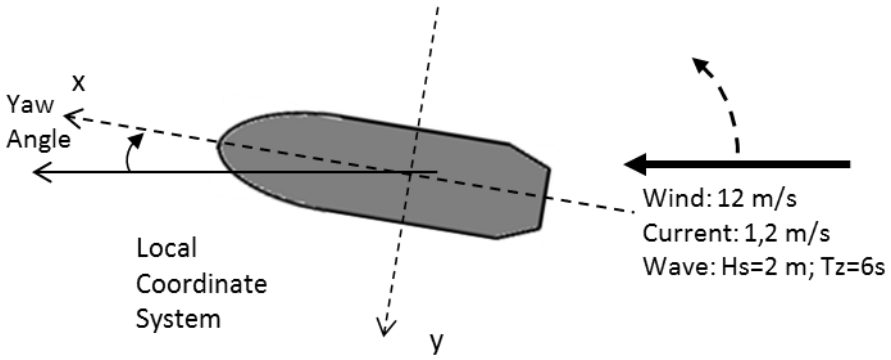

Source: Arditti, et al (2018a).

The control set point was defined at the origin of the global coordinate system (X, Y, φ_{yaw}) = (0, 0, 0°). The hydrodynamic interactions were also considered

according to the previously defined model. Again, the simulation considers the same two thrust allocation algorithms.

Figure 6. 12 presents the simulation results for both algorithms. Observe that the maximum displacement of the vessel is significantly larger when the hydrodynamic interactions are not considered (red line). In the worst case it moved almost 10 m, while the algorithm considering the hydrodynamic interactions (blue line), kept the vessel up to 2 m from the set point.

Figure 6. 12 – Maximum displacement of the vessel.

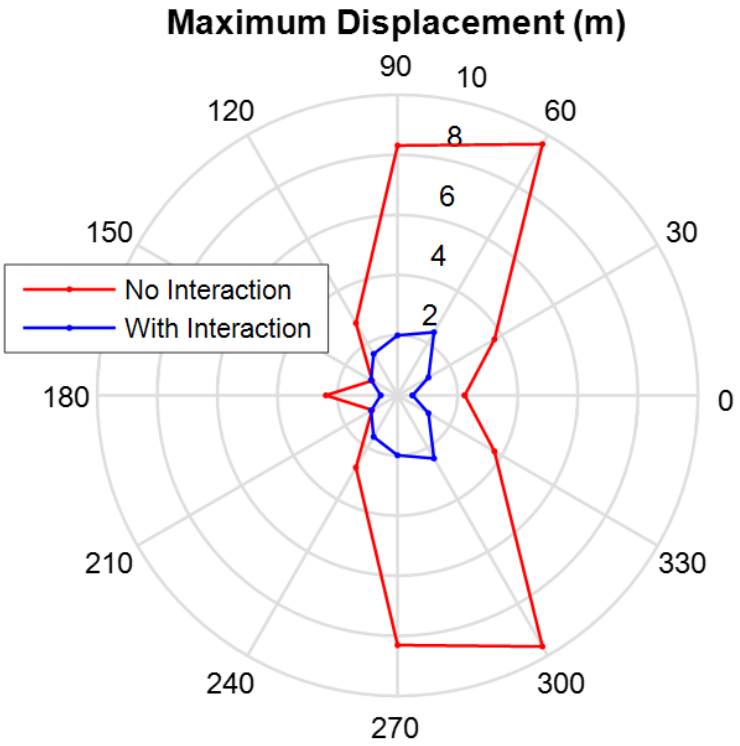

Source: Arditti, et al (2018a).

Analyzing the result of the worst case in detail on Figure 6. 13, it is clear that by accurately generating the required forces, which is only possible if the hydrodynamic interactions are considered, the vessel stays closer to the set point.

Figure 6. 13 – Vessel gravity center movements in a 2D graph.

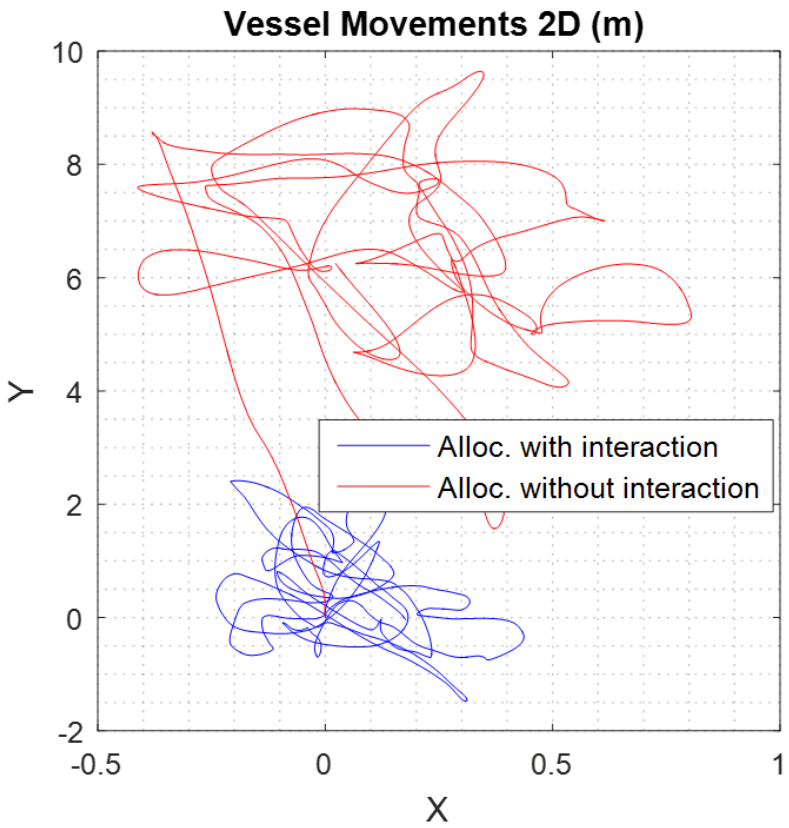

Source: Arditti, et al (2018a).

However, one disadvantage of the designed controller is that it does not contain an integral control parcel. This explains why the vessel, when not considering the hydrodynamic interaction appears to have a regime position not in the defined set point. Therefore, a different analysis is presented in Figure 6. 14 to highlight the importance of considering hydrodynamic interactions. In the following image the standard deviation of the vessel in relation to its central point (regime position) position is presented. Observe that in the cases in which the hydrodynamic interactions are not considered the standard deviation around the regime position are considerably higher (in average 75%) than the cases where the hydrodynamic interactions are considered. This happens because when the forces are not accurately generated (only possible when hydrodynamic interactions are considered), the control system does not get the expected vessel behavior and higher forces are required, leading to increased chattering around the regime (central) point.

Figure 6. 14 – Standard deviation from the regime position.

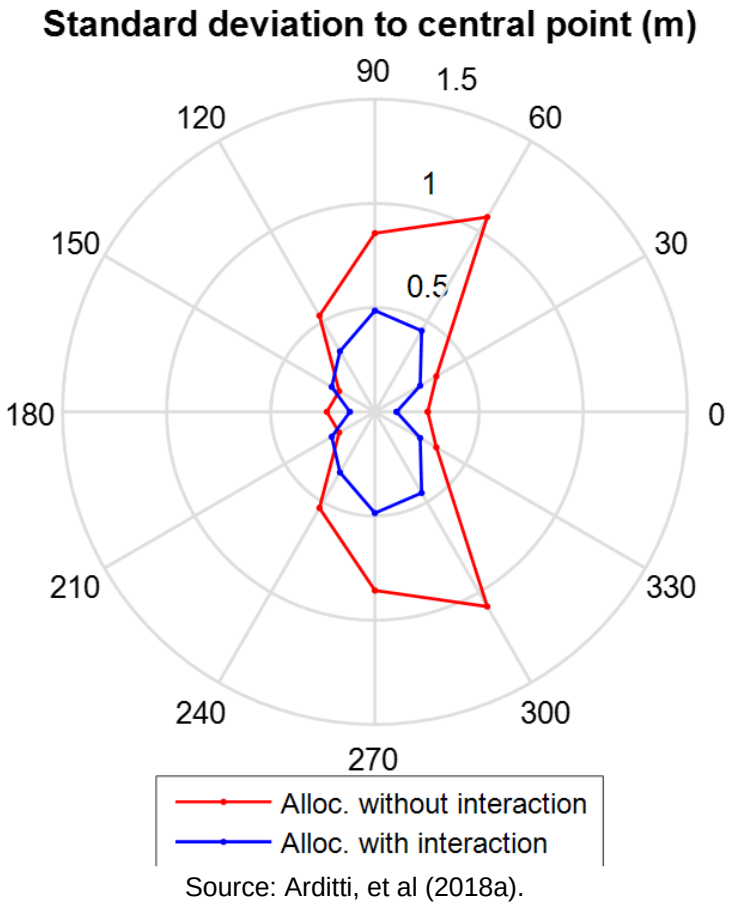

Source: Arditti, et al (2018a).

Furthermore, Figure 6. 15 presents the average power consumption of the vessel. Note that the power consumption of the algorithm that does not consider the hydrodynamic interaction is significantly higher (in average 25%) than the cases where the hydrodynamic interactions are considered. Two reasons explain this result. The first one is that by not considering the interactions, the control system may position some thrusters in conditions where they are not efficient, thus requiring more force generation to compensate. The second one is that by keeping the vessel closer to its regime position (lower standard deviation) a less aggressive control is required, since a significant part of the required forces is to compensate the error.

Figure 6. 15 – Average power consumption.

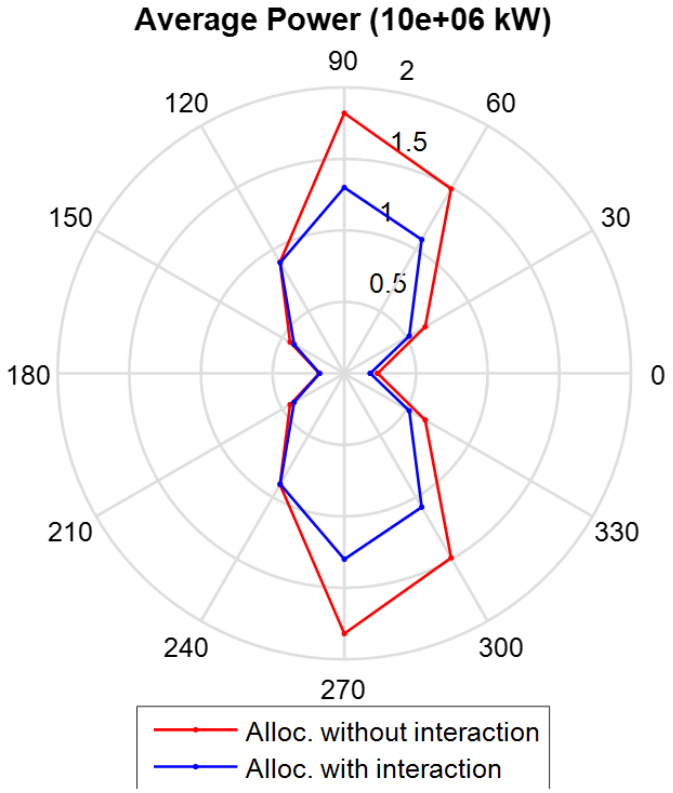

Source: Arditti, et al (2018a).

The results demonstrate the need to consider the hydrodynamic interaction effects within the thrust allocation. By doing that, the overall performance of the DP system is improved, both in controllability and in power consumption. Furthermore, better regime behavior with significantly smaller chattering around the regime position is obtained, which also reflects on better power consumption.

7. CONCLUSIONS AND FUTURE WORK

As discussed in the introduction chapter, the hydrodynamic interaction effects and physical limitations, significantly affect the thrust allocation algorithm. Therefore, modelling them is of great importance in order to improve the vessel's DP capability. Although the hydrodynamic interaction effects have been studied separately, the separation of phenomena in inflow and wake flow interaction allows fully modeling the complex hydrodynamic effects and considering them in a structured manner. Furthermore, modelling the physical limitations of the thrusters as inequality constraints allows direct implementation in the structure of optimization problems.

Additionally, representing the hydrodynamic interactions by means of efficiency functions eliminates the needs to consider forbidden zones, which brings nonlinearities to the problem and prevents a smooth control, in case the thruster needs to cross that zone.

Considering the optimization methods discussed and the structure of the optimization problem modelled, the SQP algorithm, with the slack variables, is the best algorithm candidate to solve the thrust allocation problem modelled.

The results show that the developed thrust allocation algorithm is numerically robust. If the problem was defined without the slack variables, it could lead to situations when a solution could not be find (e.g. saturation simulation), which could lead to unexpected behavior of the vessel. Therefore, the robust definition comes from the fact that the thrust allocation algorithm can handle situations where it is not possible to generate the required forces. Furthermore, in these cases it prevents the vessel from leaving the weather vane position, which could lead to higher environmental forces.

The results clearly demonstrate the need to consider the hydrodynamic interaction effects within the thrust allocation. By doing that, the overall performance of the DP system is improved, both in controllability and in power consumption.

Simulations with the vessel model, environmental conditions, complete DP system and a consistent hydrodynamic interaction model could bring improvements

to the shipbuilding industry by simulating general offshore operations (e.g. drilling assisted by DP) and complex ship maneuvering; making them more reliable

7.1. Future Work

Some suggestions for future work that can benefit from the developments of this research are presented:

- Incorporate the hydrodynamic interaction models and thrust allocation method to the simulators of TPN. The maneuver simulators of TPN already perform significantly detailed simulations taking into account numerous information from the vessel and the environment. By including the findings of this research, it would give another step to make the simulations as close to the reality.
- Model tests of the thrust allocation algorithm could be carried out in TPN basin. These tests would allow further exploring the benefits of considering hydrodynamic interactions on thrust allocation and verify how precise are the models adopted to represent them.
- Finally, incorporating all the propulsion models to the thrust allocation model could be performed. Although the modelling of main propellers and tunnel thrusters considering the wake flow interaction is straight forward, the couple main propeller and rudder is not so simple. In the appendix, a method for modelling this couple as an azimuth thruster is presented.

8. APPENDIX

8.1. Modelling Main Propeller and Rudder as an Azimuth Thruster

Motivated by the modelling of azimuth thrusters as the combination of thrust, azimuth angle and efficiency combination (inflow and wake flow). The couple main propeller and rudder is modelled as an azimuth thruster.

Initially two models for representing the force generation of the couple are presented. The first model is based on the study of the drag forces of the wake flow on the rudder, whereas the second model is based on an empirical method presented in the ABS guide (ABS 2013).

8.1.1. Main thruster and rudder force generation models

DRAG FORCES

The model for the forces generated by the couple main propeller and rudder presented in the Eq. 8.1 can be found in Johansen *et al.* (2008). T_F and T_B are the forces generated by the main propeller forward and backward, respectively. L_R are the lift forces generated by the rudder. D_R are the dragging forces generated by the rudder. n is the angular speed of the main thruster and δ is the angular position of the rudder. K_{T_F}, K_{T_B}, $K_{L\delta_1}$, $K_{L\delta_2}$, $K_{D\delta_1}$ and $K_{D\delta_2}$ are constants obtained through model tests.

$$
\begin{aligned}
T_F &= K_{T_F} \cdot n^2 && n \geq 0 \\
T_B &= K_{T_B} \cdot |n| \cdot n && n < 0 \\
L &= T_F(1 + K_{Ln} \cdot n)(K_{L\delta_1} \cdot \delta + K_{L\delta_2} \cdot |\delta| \cdot \delta) && n \geq 0 \\
L &= 0 && n < 0 \\
D &= T_F(1 + K_{Dn} \cdot n)(K_{D\delta_1} \cdot \delta + K_{D\delta_2} \cdot \delta^2) && n \geq 0 \\
D &= 0 && n < 0
\end{aligned}
\tag{8.1}
$$

Finally, the forces generated in surge and sway direction are obtained through:

$$
\begin{aligned}
F_x &= T - D \\
F_y &= L
\end{aligned}
\tag{8.2}
$$

ABS GUIDE FOR DYNAMIC POSITIONING SYSTEMS

Figure 8. 1 presents the forces generated by the couple main propeller and rudder for a high efficiency rudder. Observe that the forces are presented as a percentage of the bollard pull force generated by the main propeller.

Figure 8. 1 – Forces generated by main propeller and rudder for a high efficiency rudder.

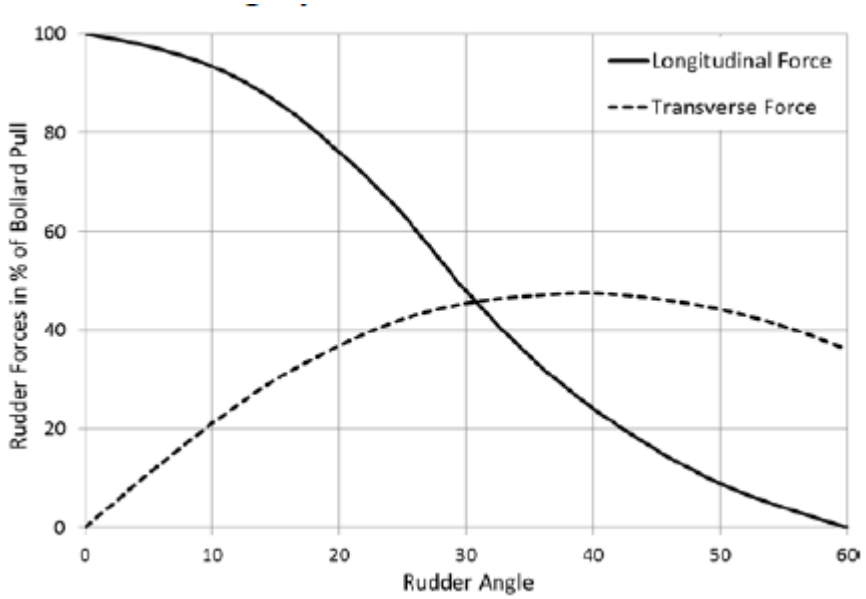

Source: ABS (2013).

Figure 8. 2 presents the thrust region of the couple main propeller and rudder based on ABS (2013) data. Note that when the force is forward, the water jet drags along the rudder allowing for forces in the sway direction. However, when the force is backwards, the rudder does not act, and it is only possible to generate forces in surge direction.

Figure 8. 2 – Thrust region of the couple main propeller and rudder.

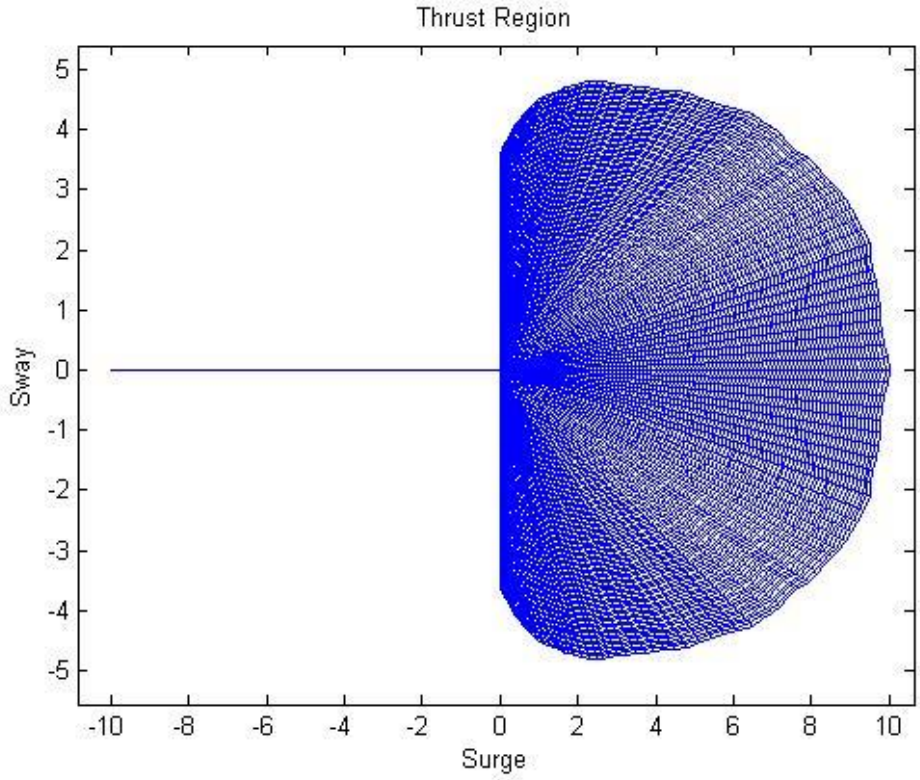

Source: Elaborated by the author.

8.1.2. Modelling with efficiency function

As observed from Figure 8. 2 the thrust region of a main propeller and rudder is similar to the thrust region of an azimuth thruster. Therefore, it can be represented as an azimuth thruster where the thrust generated by the main propeller is equivalent to the thrust generated by the azimuth thruster and the rudder angle (δ) is similar to the azimuth angle (α).

Note that δ and α are not directly equivalent because the direction of the force generated by the azimuth thruster is α, whereas the direction of the force generated by the main propeller and rudder is different from δ. Once this small difference is noted, it is easily solved in the modelling by defining different efficiency functions for surge and sway directions and by not correcting the direction of the force with senoidal functions (as it is performed for azimuth thrusters).

The result of this modelling is presented in Eq. 8.3, where T is the thrust delivered by the main propeller and $\eta_{surge}(\delta)$ and $\eta_{sway}(\delta)$ are the efficiency functions for their

respective directions. Furthermore, note that these efficiency functions are exactly the efficiencies represented in Figure 8. 1

.

$$F_x = T \cdot \eta_{surge}(\delta)$$
$$F_y = T \cdot \eta_{sway}(\delta) \tag{8.3}$$

Finally, it is important to remember that the phenomena related with the inflow of the main propeller should be considered. And the interaction with the rudder, which generates $\eta_{surge}(\delta)$ and $\eta_{sway}(\delta)$ can be seen as the wake flow interaction. Therefore, the couple main propeller and rudder is well represented by a modified azimuth thruster.

REFERENCES

ARDITTI, F. COZIJN, H. VAN DAALEN, E. F. G. 2014. An advanced thrust allocation algorithm for dp applications, taking into account interaction effects and physical limitations. *OMAE.* 2014.

ARDITTI, F. COZIJN, H. VAN DAALEN, E. F. G. TANNURI, E. A. 2018a. Dynamic Positioning simulations of a Thrust Allocation Algorithm considering Hydrodynamic Interactions. *IFAC CAMS.* 2018a.

—. 2018. Robust thrust allocation algorithm considering hydrodynamic interactions and actuator physical limitations. *Journal of Marine Science and Technology.* 2018, pp. 1-14.

ARDITTI, F. SOUZA, F. L. MARTINS, T. C. TANNURI, E. A. 2015. Thrust allocation algorithm with efficiency function dependent on the azimuth angle of the actuators. *Ocean Engineering.* 2015, Vol. 105, pp. 206-216.

ARDITTI, F. TANNURI, E. A. 2018. Dynamic Positioning Improvements by Considering Hydrodynamic Interactions. *INDUSCON.* 2018.

—. 2012. Experimental Analysis of a Thrust Allocation Algorithm for DP Systems Considering the Interference between Thrusters and Thruster-Hull. *MCMC.* 2012.

—. 2011. Thrust Allocation Algorithm for DP Systems Considering the Interference between Thrusters and Thruster-Hull. *COBEM.* 2011.

BOSLAND, R. DIJK, J. M. HUIJSMANS, R. H. M. 2009. Numerical Prediction of Thruster-thruster Interaction. *OMAE.* 2009.

CARLTON, J. S. 2007. *Marine propellers and propulsion. – 2nd ed.* s.l. : Butterworth-Heinemann, Oxford, 2007.

CONSOLIDATED TRAINING SYSTEMS INCORPORATED 2019. Available in: < http://ctsi.com.ph/index.php/look-worlds-first-carbon-fiber-main-propeller/>. Acessed in: 17 mar. 2017.

COZIJN, H. HALLMANN, R. 2013. Thruster-interaction Effects on a DP Semi-submersible and a Drill Ship - Measurements and Analysis of the Thruster Wake Flow. *OMAE.* 2013.

COZIJN, J. L. HALLMANN, R. 2012. THE WAKE FLOW BEHIND AZIMUTHING THRUSTERS: MEASUREMENTS IN OPEN WATER, UNDER A PLATE AND UNDER A BARGE. *OMAE.* 2012.

DANG, J. LAHEIJ, H. 2004. Hydrodynamic Aspects of Steerable Thrusters. *Dynamic Positioning Conference.* 2004.

DA-WEI, Z. FU-GUANG, D. JIN-FENG, T. YUE-QIANG, L. XIN-QIAN, B. 2010. Optimal thrust allocation based GA for dynamic positioning ship. *IEEE International Conference on Mechatronics and Automation.* 2010.

DE WIT, C. 2009. Optimal Thrust Allocation Methods for Dynamic Positioning of Ships. *Delft Univerisity of Technology - MSC Thesis.* 2009.

DING, F. YANG, D. HUANG, W. 2016. Study on stabilizing power of dynamic positioning ship based on thrust allocation. *IEEE International Conference on Mechatronics and Automation.* 2016.

DNV. 2016. ST-0111- Standard for Assessment of station keeping capability of dynamic positioning vessels. 2016.

EKSTROM, L. BROWN, D. T. 2002. Interactions Between Thrusters Attached to a Vessel Hull. *OMAE.* 2002.

GIERUSZ, W. TOMERA, M. 2006. Logic Thrust Allocation Applied to Multivariable Control of Training Ship. *Control Engineering Practice.* 2006, Vol. 14, pp. 511-524.

GRANJA, B.B. MADUREIRA, R. M. L. TANNURI, E. A. 2010. Alocação de Empuxo Para Sistema DP: Efeito da Utilização de Lemes de Alto Desempenho. *23º Congresso Nacional de Transporte Aquaviário, Construção Naval e Offshore (SOBEMA).* 2010.

HISEA MARINE 2019. Available in: < http://www.hiseamarine.com/marine-azimuth-thruster-1090.html>. Acessed in: 17 mar. 2019.

JENSSEN, N. A. REALFSEN, B. 2006. Power Optimal Thruster Allocation. *Dynamic Postioning Conference.* 2006.

JOHANSEN, T. A. FOSSEN, T. I. BERGE, S. P. 2004. Constrained Nonlinear Control Allocation with Singularity Avoidance using Sequential Quadratic Programming. *IEEE Transactions on Control Systems Technology.* 1, 2004, Vol. 12, pp. 211-216.

JOHANSEN, T. A. FOSSEN, T. I. 2013. Control allocation - a survey. *Automatica.* 5, 2013, Vol. 49, pp. 1087-1103.

JOHANSEN, T. A. FUGLSETH, T. P. TØNDEL, P. FOSSEN, T.I. 2008. Optimal Constrained Control Allocation in Marine Surface Vessel with Rudders. *Control Engineering Practice.* 2008, Vol. 16, pp. 457-464.

JOHANSEN, T. A., FOSSEN, T. I. TØNDEL, P. 2005. Efficient Optimal Constrained Control Allocation via Multi-Parametric Programming. *AIAA Journal of Gudance, Control and Dynamics.* 2005, Vol. 28, pp. 506-515.

JÜRGENS, D. PALM, M. AMELANG, A. MOLTRECHT, T. 2008. Design of Reliable Steerable Thrusters by Enhanced Numerical Methods and Full Scale Optimization of Thruster-Hull Interaction Using CFD. *MTS DP Conference.* 2008.

KARLSEN, A. PIVANO, L. RUTH E. 2016. DNV GL DP Capability-A New Standard for Assessment of the Station-Keeping Capability of DP Vessels. *Marine Technology Society (MTS) DP Conference.* 2016.

KJERSTAD, Ø. K. SKJETNE, R. BERGE, B. O. 2013. Constrained Nullspace-Based Thrust Allocation for Heading Prioritized Stationkeeping of Offshore Vessels in Ice.

International Conference on Port and Ocean Engineering under Arctic Conditions (POAC). 2013.

KONGSBERG 2019. Available in: < https://www.km.kongsberg.com/ks/web/nokbg0238.nsf/AllWeb/FDC6B7B44712AC6CC125789B00324141?OpenDocument >. Acessed in: 17 mar. 2019.

LIANG, C. C. CHENG, W. H. 2004. The Optimal Control of Thruster System for Dynamically Positioned Vessels. *Ocean Engineering.* 2004, Vol. 31, pp. 97-110.

MARINE INSIGHT 2019. Available in: < https://www.marineinsight.com/marine-navigation/how-bow-thruster-is-used-for-maneuvering-a-ship/>. Acessed in: 17 mar. 2019.

MAURO, F. NABERGOJ, R. 2016. Advantages and disadvantages of thruster allocation procedures in preliminary dynamic positioning predictions. *Ocean Engineering.* 2016, Vol. 123, pp. 96-102.

MOBERG, HELLSTRÕM, S. A. 1983. Dynamic Positioning of a four column semi-submersible. Model testes of interaction forces and a philosophy about optimum strategy when operating thrusters. *Proceedings of second International Symposium on Ocean Engineering and Ship Handling.* 1983.

NISHIMOTO, K., FUCATU, C.H., MASETTI, I.Q. 2002. DYNASIM - A Time Domain Simulator of Anchored FPSO. *Journal of Offshore Mechanics Arctic Engineering ASME.* 124, 2002, pp. 1-9.

NOCEDAL, J. WRIGHT, S. J. 2006. Numerical Optimization. *Second Edition.* Springer, 2006.

PALM, M. JÜRGENS, D. BENDL, D. 2010. Comparison of Thruster Axis Tilting versus Nozzle Tilting on the Propeller-hull Interactions for a Drillship at DP-conditions. *MTS DP Conference.* 2010.

PALMER, A. R. HEARN, G. E. STEVENSON, P. 2009. Thruster Interactions on Autonomous Underwater Vehicles. *OMAE.* 2009.

RINDARØY, M. 2013. Fuel Optimal Thrust Allocation in Dynamic Positioning. *Master degree thesis. Institutt for Teknisk Kybernetikk, Norway.* 2013.

RUTH, E. SØRENSEN, A. J. PEREZ, T. 2007. Thrust allocation with linear constrained quadratic cost function. *IFAC Conference on Control Applications in Marine Systems.* 2007.

SERRARIS, J. J. 2009. Time-domain Analysis for DP Simulations. *OMAE.* 2009.

SHI-ZHI, Y. WANG, L. SUN, P. 2011. Optimal thrust allocation logic design of dynamic positioning with pseudo-inverse method. *Journal of Shanghai Jiaotong University.* 2011, Vol. 16, pp. 118–123.

SILVA, E. C. N. 2011. Otimização Aplicada ao Projeto de Sistemas Mecânicos. *Apostila do curso de Otimização Aplicada ao Projeto de Sistemas Mecânicos (PMR*

5215), oferecido no curso de Engenharia Mecatrônica da Escola Politécnica da USP. 2011.

SKJETNE, R. KJERSTAD, Ø. K. 2013. Recursive nullspace-based control allocation with strict prioritization for marine craft. *IFAC Conference on Control Applications in Marine Systems.* 2013.

SLOTINE, J. E. LI, W. 1991. *Applied Nonlinear Control.* s.l. : Prentice Hall, 1991.

SORDALEN, O. J. 1997. Optimal thrust allocation for marine vessels. *Control Engineering Practice.* 1997, Vol. 5, pp. 1223-1231.

SORENSEN, A. J. 2011. A survey of dynamic positioning control systems. *Annual Reviews in Control.* 1, 2011, Vol. 35, pp. 123-136.

TANNURI, E. A. 2002. Desenvolvimento de Metodologia de Projeto de Sistema de Posicionamento Dinamico Aplicado a Operaçoes em Alto-Mar. *Tese de Doutorado – Escola Politécnica da USP.* 2002.

TANNURI, E. A. MORISHITA, H. M. 2006. Experimental and Numerical Evaluation of a Typical Dynamic Positioning System. *Applied Ocean Research.* 2006, Vol. 28, pp. 133-146.

TANNURI, E. A. PESCE, C. P. ALVES, G. S. MASETTI, I. RIBAS FERREIRA, P.P. 2002. Dynamic Positioning of a Pipeline Launching Barge. *International Offshore and Polar Engineering Conference.* 2002.

TANNURI, E.A., PESCE, C.P., ALVES, G.S., MASETTI, I.Q., RIBAS FERREIRA, P.P. 2002. Dynamic Positioning of a Pipeline Launching Barge. *The Twelfth International Offshore and Polar Engineering Conference. International Society of Offshore and Polar Engineers.* 2002.

TANNURI, E.A., SAAD, A.C., MORISHITA, H.M. 2009. Offloading Operation with a DP Shuttle Tanker: Comparison Between Full Scale Measurements and Numerical Simulation Results. *8th Conference on Manoeuvring and Control of Marine Craft (MCMC).* 2009.

Thrustmaster of Texas, Inc. Techincal Specification (private document): Model OD-2000N Hydraulic Outboard Thruster Unit.

VAN DAALEN, E. F. G. COZIJN, H. LOUSSOUARN, C. HEMKER, P. W. 2011. A generic optimization algorithm for the allocation of DP actuators. *OMAE.* 2011.

VAN DIJK, R. R. T. AALBERS, A. B. 2001. What happens in water the use of hydro-dynamics to improve DP. *MTS Dynamic Positioning Conference.* 2001.

VEKSLER, A. JOHANSEN, T. A. BORRELLI, F. REALFSEN, B. 2016. Dynamic Positioning With Model Predictive Control. *IEEE TRANSACTIONS ON CONTROL SYSTEMS TECHNOLOGY.* 2016, Vol. 24, pp. 1340-1353.

VEKSLER, A. JOHANSEN, T. A. SKJETNE, R. MATHIESEN, E. 2015. Thrust Allocation With Dynamic Power Consumption Modulation for Diesel-Electric Ships. *IEEE TRANSACTIONS ON CONTROL SYSTEMS TECHNOLOGY.* 2015, Vol. 24, pp. 578-593.

VEKSLER, A. JOHANSEN, T. A. SKJETNE, R. 2012. Thrust allocation with power management functionality on dynamically positioned vessels. *American Control Conference.* 2012.

WEBSTER, W. C. SOUSA, J. 1999. Optimum Allocation for Multiple Thrusters. *ISOPE Conference.* 1999.

WEI, Y. FU, M. NING, X. SUN, X. 2013. Quadratic programming thrust allocation and management for dynamic positioning ships. *TELKOMNIKA.* 2013, Vol. 11, pp. 1632-1638.

WEN, W. XU, H. FENG, H. 2016. Research on Thrust Allocation Algorithm Based on Group Biasing Strategy. *International Ocean and Polar Engineering Conference.* 2016.

WU, D. REN, F. ZHANG, W. 2016. An energy optimal thrust allocation method for the marine dynamic positioning system based on adaptive hybrid artificial bee colony algorithm. *Ocean Engineering.* 2016, Vol. 118, pp. 216-226.

XU, S. WANG, X. WANG, L. LI, B. A. 2016. Dynamic Forbidden Sector Skipping Strategy in Thrust Allocation for Marine Vessels. *International Journal of Offshore and Polar Engineering.* 2016, Vol. 26, pp. 1-8.